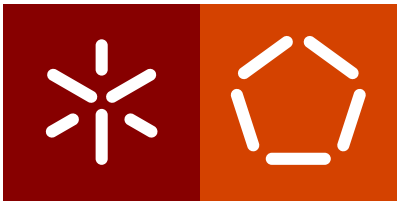

Universidade do Minho
Escola de Engenharia
Departamento de Eletrónica Industrial

Ricardo Nuno Sousa Guimarães

Wearable muscle force sensory system-MuscLab

September 2018

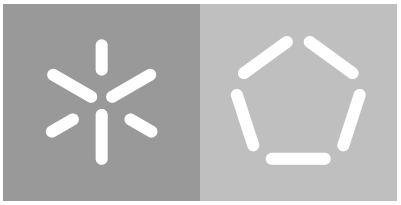

Universidade do Minho
Escola de Engenharia
Departamento de Eletrónica Industrial

Ricardo Nuno Sousa Guimarães

Wearable muscle force sensory system-MuscLab

Master dissertation
Master Degree in Industrial Eletronics and Computers

Dissertation supervised by
Professora Doutora Cristina P. Santos

September 2018

ACKNOWLEDGEMENTS

This dissertation would not be possible without the aid of some people worth of being mentioned.

First of all, I would like to thank my mentor Dr. Cristina P. Santos for the amazing opportunity of letting me work under her supervision in the area of medical rehabilitation. It was through your teachings and methods that I learnt how to become a more capable person.

I would also like to thank my colleague Joana Figueiredo, for the opportunity to work with her and for her endless support. I can't even express how much I grew as a person and professional by your side.

For all the laboratory staff members, thank you for all the moments spent in there and for providing an excellent place for work. Thank you for letting me be a part of this incredible team.

To the workshop staff, Ângela Maria, Joel Almeida and Carlos Torres, thank you for saving me from my problems every time and for our interesting talks and share of wisdom. Thank you guys, you will never be forgotten.

To my friends that joined me in this journey along the university, specially Chuck, Jomi, Diogo, David, Rita, Pedro, Bino, Almeida, João Alves, Bruno Sousa, Hélder Freitas and Pedro Santos, for all the moments we shared and for the strong relationships I know that will endure.

To my team mates in Vitória Sport Clube, thank you for all the moments spent and for helping me grow up as a person through this long journey. To my close mentors António, Nelson, Pastor and Daniele, part of who I am today is because of you guys, thank you very much.

To my life time friends and family in Guimarães, thank you for everything and for your aid in the good and bad moments. You were seriously a crucial part of this.

Finally and the most important, mom and dad, this one is for you. All of what I am, and all I have and will achieve, I will because of you guys and your education, efforts and sacrifices. Thank you for turning me into the man I am today.

ABSTRACT

Sarcopenia, the age-associated loss of skeletal muscle mass, has been postulated to be a major factor in the strength decline with ageing. Considering the increase in the number of people with muscle weakness, the monitoring of a person's muscular activity becomes a necessity. This need is also present in the sports area, since the muscles monitoring allows an improvement in the athlete's technique and may also help preventing possible injuries.

The standard method for muscle monitoring is the electromyography signal acquisition, although it presents various problems, like their lack of ergonomics, requiring hairless skin and gel inserted in it, and the need of complex electronics, demanding several hardware filters, since the EMG raw data is full of noise.

This dissertation consists in developing a wearable prototype to monitor the user's muscular activity, through force sensing resistors sensors, and recognize the toe-off gait event. The sensors data are processed by a microcontroller and are sent to a desktop application through wireless connection, or saved in a memory card for a later analysis. This project was also integrated in the robotic system SmartOs.

The force sensors output signals were validated by comparing them to the EMG signals. These trials were divided in two groups: static trials, in which the subjects performs specific gestures several times, and dynamic trials, where the subject walks in different paces (slow, medium and fast). Both signals showed some similarity between them, although their similarities were more obvious in the static trials because of their more simple and linear signals. Several regression methods were validated in order to convert the FSR in EMG signals, but the results showed poor results, discarding this possible implementation. The gait event toe-off recognition algorithm was also validated in the dynamic trials performed. The results were satisfactory, showing a high accuracy percentage and low delay times.

This dissertation project should provide an easier way to monitor muscles, discarding the needs of complex electronics and hairless skin and providing a clean signal with few noise.

Keywords: *Muscle weakness; Monitoring; Muscular activity; Human motion; Detection; Recognition; Force Sensors;*

RESUMO

Sarcopenia, a perda de massa muscular esquelética associada à idade, tem sido postulada como um fator importante no declínio de força com o envelhecimento. Com o aumento do número de pessoas com fraqueza muscular, uma monitorização da atividade muscular de uma pessoa torna-se uma necessidade. Esta necessidade também está presente na área do desporto, em que a monitorização muscular permite uma melhoria na técnica do atleta ou prevenir possíveis lesões.

O método padrão para a monitorização muscular é a aquisição do sinal EMG, embora apresente vários problemas, como a sua falta de ergonomia, exigindo pele depilada e inserção dum gel específico, e a necessidade de eletrónica complexa, composta por vários filtros, uma vez que os sinais EMG contém muito ruído.

Esta dissertação consiste em desenvolver um protótipo vestível para monitorizar a atividade muscular do utilizador através de sensores piezoresistivos e reconhecer o evento da marcha *toe-off*. Os dados dos sensores são processados por um microcontrolador que envia os dados para uma aplicação gráfica por comunicação *wireless* ou então são guardados num cartão de memória para uma futura análise. Este sistema também foi integrado no sistema robótico SmartOs.

Os sinais provenientes dos sensores de força foram validados, comparando-os com os sinais EMG. Estes testes foram divididos em dois grupos: testes estáticos, onde a pessoa realiza movimentos específicos repetidamente, e testes dinâmicos, onde a pessoa caminha em diferentes velocidades (lenta, média e rápida). Os testes mostraram alguma semelhança entre os dois sinais, embora estas semelhanças foram mais visíveis nos testes estáticos devido ao facto dos seus sinais serem mais simples e lineares que nos testes dinâmicos. O algoritmo de reconhecimento do evento *toe-off* foi validado nos testes dinâmicos realizados, mostrando resultados satisfatórios tais como altas percentagens de precisão e curtos atrasos temporais.

Este projeto deverá fornecer uma maneira mais fácil de monitorizar os músculos, não necessitando de eletrónica complexa ou de ter a pele depilada e a inserção de gel, fornecendo assim um sinal livre de muito ruído.

Keywords: *Fraqueza muscular; Monitorização; Atividade muscular; Movimentos humanos; Deteção; Reconhecimento; Sensores de força;*

CONTENTS

LIST OF FIGURES

LIST OF TABLES

ACRONYMS

AC Alternating Current. 20
ADC Analog-to-Digital Converter. 37, 46, 53, 62
ARM Advanced RISC Machine. 42, 59

CAD Computer Aided Design. 49
CAR Control, Automation and Robotics. 1
CMEMS Center for Microelectromechanical Systems. 1, 61
CPU Central Processing Unit. 59, 60

DAQ Data Acquisition. 17
DC Direct Current. 20
DEI Departamento de Eletrónica Industrial. 1
DFT Discrete Fourier Transformation. 48

ELM Extreme Learning Machine. 33
EMG Electromyography. 2, 3, 12–15, 21, 23–26, 48, 61–63, 65, 67, 68, 70–75, 78–80
EPAD Exoskeletal Power Assistive Device. 24

FADEUP Faculdade de Desporto da Universidade do Porto. 61
FC Foot Contact. 31
FIR Finite Impulse Response. 29
FMG Force Myographic. 17
FO Foot Off. 31
FPCB Flexible Printed Circuit Board. 80
FSR Force Sensing Resistor. 7–17, 26, 29, 33, 34, 37, 38, 43, 44, 46–48, 50, 53, 54, 56, 61–63, 65, 67, 68, 70–75, 77–80

GUI Graphical User Interface. 3, 4, 37, 51, 53, 56–58, 60, 77
GWFs Graphene Woven Fabrics. 25, 26

HMM Hidden Markov Models. 31

IDE Integrated Development Environment. 51, 57

IMU Inertial Measurement Unit. 21, 23
ISR Interrupt Service Routine. 52

kNN k-Nearest-Neighbor. 30, 31

LABIOMEP Laboratório de Biomecânica do Porto. 61, 67, 68
LDA Linear Discriminant Analysis. 32

MCU Microcontroller Unit. 4, 37, 38, 41, 43, 45, 46, 51–53, 57–60, 63, 77
MFE Muscle Fiber Expansion. 23–25
MIEEIC Mestrado Integrado em Engenharia Eletrónica Industrial e Computadores. 1
MMG Mechanomyogram. 2, 3
MSF Muscular Stiffness Force. 8, 9
MVC Maximum Voluntary Contraction. 23, 28

PCB Printed Circuit Board. 4, 48, 50, 62, 63, 77, 80
PDMS polydimethylsiloxane. 25
PID Proportional–Integral–Derivative. 29, 30
pMMG pressure-based MMG. 22, 23, 28
PTF Polymer Thick Film. 8
PVC Polyvinyl Chloride. 22

QML Qt Modeling Language. 57

RAM Random Access Memory. 59
RMS Root Mean Square. 20
RMSE Root Mean Square Error. 65–67, 69, 70, 78

SDIO Secure Digital Input Output. 44
sEMG surface Electromyography. 9
SNR Signal to Noise Ratio. 22
SPI Serial Peripheral Interface. 38, 44
SVR Support Vector Regression. 72, 73, 78

TD Time-Domain. 32

UM Universidade do Minho. 1

VI Vastus Intermedius. 8, 9
VL Vastus Lateralis. 8

1

INTRODUCTION

This dissertation was developed in the *Mestrado Integrado em Engenharia Eletrónica Industrial e Computadores (MIEEIC)* in the *Departamento de Eletrónica Industrial (DEI)* of the *Universidade do Minho (UM)*, more specifically in the branch *Control, Automation and Robotics (CAR)*, in the area of medical rehabilitation in the *Center for Microelectromechanical Systems (CMEMS)* laboratory. This dissertation is also integrated in the *SmartOS* project.

In this chapter it will be presented the motivation behind this dissertation, as well as a problem statement, explaining the existing problems in this society and solutions available for trying to answer the existing needs, and finally the possible contributions of this project. Later, it will be presented a list of this dissertation goals and research questions, as well as the structure of this document.

1.1 MOTIVATION

Muscle weakness is consistently reported as an independent risk factor for high mortality in older adults. Since muscle strength also appears to be a critical component in maintaining physical function, mobility, and vitality in old age, it is paramount to identify factors that contribute to the loss of strength in elderly persons. Sarcopenia, the age-associated loss of skeletal muscle mass, has been postulated to be a major factor in the strength decline with ageing. Moreover, sarcopenia is related to functional impairment, disability, falls, and loss of independence in older adults (Goodpaster et al., 2006). Using the estimate providing the lowest prevalence estimates, the number of individuals with sarcopenia would rise in Europe from 10,869,527 in 2016 to 18,735,173 in 2045 (a 72.4% increase). This corresponds to an overall prevalence of sarcopenia in the elderly rising from 11.1% in 2016 to 12.9% in 2045. With the definition providing the highest prevalence estimates, the number of individuals with sarcopenia would rise from 19,740,527 in 2016 to 32,338,990 in 2045 (a 63.8% increase),

corresponding to overall prevalence rates in the elderly of 20.2% and 22.3% for 2016 and 2045, respectively. This showed that the number of sarcopenic patients will dramatically increase in the next 30 years, making consequences of muscle wasting a major public health issue (Ethgen et al., 2017).

1.2 PROBLEM STATEMENT

Considering this increase in the number of people with muscle weakness, the monitoring of a person's muscular activity becomes a necessity in these days. Monitoring muscle activity is widely practiced in medicine and sports, for the evaluation of an athlete muscular status, as well as the improvement of his motion technique. The scientific standard technique for this monitoring is called *Electromyography (EMG)*. It relies on a pair of electrodes placed at specific locations on the surface of the muscle belly. EMG is a rich and reliable source of information about muscle activity by detecting the electromechanical properties of muscle fibres. However, since the electrical potentials that it measures are very faint, it requires careful electrode placement and excellent contact with the skin, demanding a better study of the muscle anatomy. In general, EMG electrodes require a specific glue in order to attach to the skin, which must be hairless. In some cases even small needles are used. In addition, complex signal processing is needed to make sense of the signals, which contain lots of noise, so the EMG devices are bulky and expensive. In summary they are not suitable for typical pervasive applications.

The second tool for monitoring muscle activity is the *Mechanomyogram (MMG)* technique. While EMG comprises the sum of the electrical contributions, the MMG signals (using vibration transducer, such as accelerometer or piezoelectric crystal contact sensors) present the mechanical oscillation that is detectable over a contracting muscle by attaching electrodes on the skin overlying the target muscle (Lukowicz et al., 2009). To solve these problems, a new method more practical is needed to monitor the muscular activity.

Wearable systems have the potential to lead to significant improvements in monitoring technology. A great benefit is the possibility of seamlessly integrating sensors and complex electronics in accessories and clothing. Wearable integration techniques such as advanced electronic packaging, embedded microsystems and functional textiles make sure that a monitoring system is not perceived as a burden and does not interfere with everyday activities (Lukowicz et al., 2004).

Concerning to the necessities of these days, a new approach for monitoring the muscle activity is needed. This dissertation will try to answer to the disadvantages of the EMG and MMG signal acquisition, discarding the need of electrodes, allowing to monitor the muscle activity without applying a specific glue to the skin, and discarding also the need of implementing a robust and expensive electronics to integrate the sensors. The solution will also be a wearable system, allowing it to be practical and ergonomic by its accessibility to wear it on and off.

1.3 GOALS AND RESEARCH QUESTIONS

This dissertation main focus is to study and develop a wearable system for monitoring a person's muscular activity. Several objectives were also proposed, as the following ones:

- **Goal 1:** To develop an ergonomic and adaptive prototype that can monitor the muscular activity of each person.
- **Goal 2:** To monitor the subject's muscular activity by saving the data in a memory card and develop a *Graphical User Interface (GUI)* for a desktop application in order to allow the monitoring in real-time.
- **Goal 3:** To detect and recognize specific gait events.
- **Goal 4:** To validate the system signals and recognition algorithm through several experiments, with the subject doing specific motions and walking.
- **Goal 5:** To function as a stand-alone product and to be integrated in another robotic system (*SmartOs*).

Among these goals, this dissertation will try to answer for the following research questions:

- **RQ 1:** Can the force sensors provide valid information to monitor muscle activity?
- **RQ 2:** Is it possible to detect and recognize gait events through muscle activity provided from the force sensors?

In order to achieve the proposed goals, several stages must be achieved in order to successfully fulfil those goals. The stages proposed are the following ones:

- **Stage 1:** Study previous works regarding which sensors and muscles were used to monitor muscular activity and motion recognition algorithms.
- **Stage 2:** From the works studied *Stage 1* choose the sensors to be used.
- **Stage 3:** Study the system architecture and its requirements, such as hardware components.
- **Stage 4:** Design and develop the hardware interface to integrate the sensor in the system and connect it to the *Microcontroller Unit (MCU)*.
- **Stage 5:** Program the microcontroller in order to receive data from the sensors and save it in a memory card or print it to a desktop application.
- **Stage 6:** Develop a software signal calibration method in the MCU.
- **Stage 7:** Choose the target limbs to be monitored by studying their influence during a person's gait.
- **Stage 8:** Design and develop *Printed Circuit Board (PCB)*s.
- **Stage 9:** Develop a specific gait event algorithm and implement it in the MCU.
- **Stage 10:** Develop a GUI for a desktop application that allows the monitoring of the subject's muscular activity in real-time. The application will be developed in Qt, in C++ language.
- **Stage 11:** Validate the system muscle monitoring signals through a customized validation protocol. First validate it in static trials, where the subject performs specific motions and analyse the muscles responsible for those actions. Then validate the system while the subject is walking.
- **Stage 12:** Validate the gait event recognition algorithm through the dynamic trials performed in *Stage 11*.
- **Stage 13:** Elaborate the conclusions from this work, according to the final validation results.

1.4 REPORT STRUCTURE

This dissertation is divided in several chapters. In Chapter 2 a state of the art is presented, showing related projects and conclusions taken from those works. In

Chapter 3 is presented a problem analysis, explaining some theoretical concepts and there is also available a brief explanation about the *SmartOs* and *MuscLab* systems, including its system overview. Chapter 4 and Chapter 5 explain the hardware and software design and development phases. Chapter 6 presents the system validation protocols and their respective results. This documents ends with Chapter 7, where several conclusions are discussed from this dissertation and the answers to the research questions, and possible future work that can be developed in order to improve this project.

2

STATE OF THE ART

To better understand the work that has already been done in the area of muscular monitoring, several projects which tried to respond to the existing needs were studied. With these studies, it can be studied which sensors can be used and their performance, and algorithms to detect and recognize human motions performed. This chapter describes the projects studied, which are divided in two categories, such as the sensory system used for the muscle monitoring and existing methods of recognizing human motion. In the end, a conclusion from this state of art is made, comparing the different sensors studied and different motions recognition algorithms.

2.1 SENSORY SYSTEM FOR MUSCLE MONITORING

By investigating projects regarding the muscle monitoring, several sensors and their attachment techniques can be used. The most common one used are the *Force Sensing Resistor (FSR)* sensors. This section is divided by the different types of sensors used, such as the FSR sensors, the capacitive sensors and others.

2.1.1 *Force Sensing Resistor*

The FSR can be defined as a special type of resistor, which resistance can be varied by varying the force or pressure applied to it. The FSR sensors are made of conductive polymer which has a property of changing its resistance based on the force applied to its surface.

Even though there are various types of force sensors, the FSR have several advantages, such as thin size (less than 0.5mm), very low cost and also good shock resistance. The only disadvantage of FSR sensors is low precision, as there will be approximately 10% or more difference in measurement results.

Force sensing resistors are called as *Polymer Thick Film (PTF)* devices. The resistance of FSR sensors decreases with increase in pressure applied to its surface (ELPROCUS, 2017).

Kim et al. (2013) used methods of a feedback control using the muscular stiffness force signal to aid an exoskeleton, which is also pretended in this dissertation. These methods are represented in a block diagram of Figure 1.

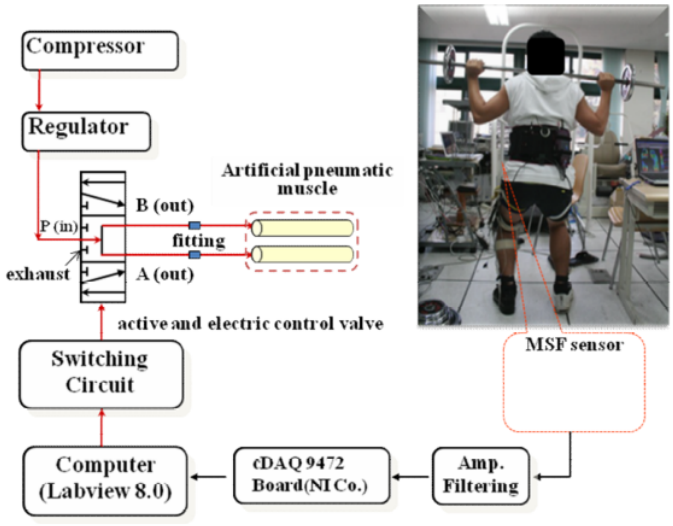

Figure 1: Block diagram of feedback control using muscular stiffness force signal (Kim et al., 2013).

According to this, two artificial pneumatic actuators which were implanted in a knee orthosis are controlled by a solenoid valve. The air pressure generated by a compressor is controlled by a regulator and it is transferred to an artificial pneumatic actuator with an action of solenoid valve. The assistance of the movement by a knee orthosis measures the *Muscular Stiffness Force (MSF)* signal, through piezoelectric resistive pressure sensors that can detect the stiffness of a muscle mainly related to the knee extension motion, which is mainly generated in the lower extremities and thereby controls the voltage of a solenoid valve with it.

The signals indicating the magnitude of muscular strength whose status can easily be detected were used. During the extension of knee joint, the contraction pressure due to the muscular activity is measured. At this time, a piezoelectric resistive pressure sensor is attached to a calf band and then closely adhered to the surface of muscles which are measured. The muscles studied and monitored were the *Vastus Lateralis (VL)* muscle and *Vastus Intermedius (VI)* muscle. A comparison was made for signals

indicating the magnitude of MSF of VI muscle and its *surface Electromyography (sEMG)* signals which were measured on an MSF sensor during the extension of knee joint. Figure 2 is a graph which was plotted following the comparative measurement of sEMG of VI muscle and the magnitude of its muscular strength during the flexion and extension of knee joint.

Accordingly, with the use of a sensor measuring the magnitude of MSF which was prepared for the current study, it was confirmed that a knee orthosis could receive a feedback control. This dissertation project will also study the contraction of other muscles, and their influence while the subject is walking.

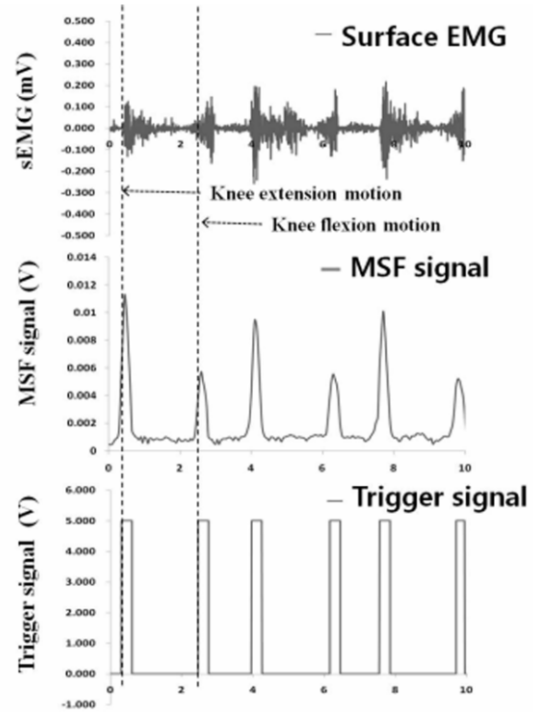

Figure 2: Synchronization of surface electromyography and muscular stiffness force signal (Kim et al., 2013).

Beil et al. (2015) developed a force sensor system for capturing interaction forces between the new lower limb exoskeleton with series elastic actuators and the human body. To measure interaction forces between exoskeleton and user as well as to determine muscular contraction, which is one of this dissertation mains goals, FSR are used. These sensors have a flat surface and small size which allow their integration in narrow spaces. As recommended by the sensor manufacturer (IEE S.A., Luxembourg) an interface was developed providing a flat and rigid mounting surface made by a

rapid prototyping technique. For a reliable coupling of forces onto the active sensing area of the FSR, a thin elastomeric layer is used. This layer fits on the active area of the sensor and avoids inhomogeneities by distributing and smoothing the pressure to the overall surface though ensuring a correct force measurement. To achieve a fast response of the exoskeleton to the user's movement, the muscular contraction of specific thigh muscles is observed. By measuring the level of muscular activity it is possible to implement a force augmentation. A value of muscular contraction (of thigh muscles) can be obtained by measuring a force signal perpendicular to the muscle. This signal is produced 0.3 s prior the movement referred to the muscular activity.

The sensor setup is illustrated in Figure 3. Placing the FSRs on top of the muscle bellies of the *rectus femoris* (S1) and *biceps femoris* (S2) provide enough information to identify the user's movement. During free swing motions the muscle activation is low.Therefore FSRs are mounted on the top end of the exoskeleton frame (S3) and at the *achilles* tendon (S4). The signals represent mainly the interaction force and facilitates free movements of the user in cooperation with the exoskeleton. Last two sensors (S5 and S6) at the bottom of the shoe underneath the heel detect contact events with the ground.

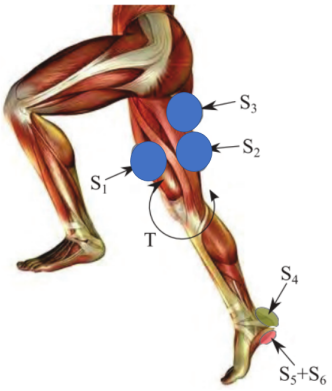

Figure 3: Setup of the sensor system; S1-S6: FSR Sensors measuring the interaction forces between user and exoskeleton Adapted. (Beil et al., 2015).

To avoid shear movements to the sensors and to amplify the force acting on the sensor, appropriate interfaces were developed. These interfaces transmit only forces perpendicular to the active area of the sensors by guiding this movement. The interfaces used for the sensors at the thigh muscles provide additional lugs to attach them easily to the Velcro straps as shown in Figure 4. The 40×40 mm^2 sized contact

surface is reduced on the rear side to get only in contact with the active area of the FSR. Since this dissertation aims also to monitor the subject's muscular activity without the aid of an exoskeleton, the FSR sensors must capture the muscles contractions and not their interactions with the exoskeleton.

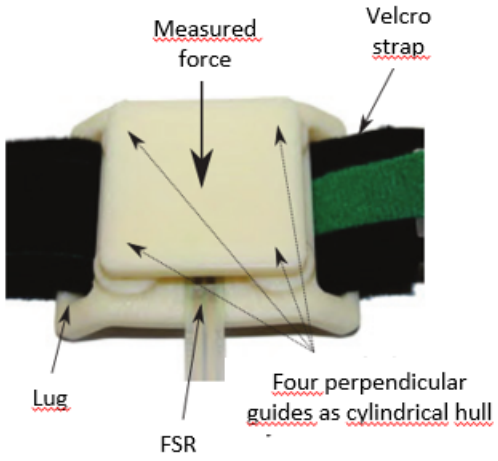

Figure 4: Design of the muscle sensor interface providing lugs for attachment to the Velcro straps Adapted (Beil et al., 2015).

Lukowicz et al. (2009) presented a system for assessing muscle activity by using wearable force sensors placed on the muscle surface.

They proposed to detect the shape changes by attaching force sensors integrated in tight fitting garments or elastic bands to the surface of the relevant muscles. The employed setup is demonstrated in Figure 5.

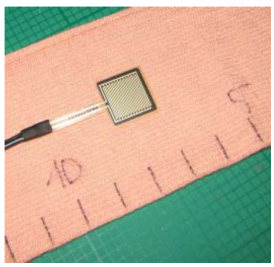

(a) The force sensor and the elastic band used in the experiments.

(b) One of the subjects with the band on the leg doing squats.

Figure 5: Lukowicz et al. (2009) FSR System (Lukowicz et al., 2009).

The FSR used was the FSR-153NS device from Conrad Electronics. It is 0.09 mm thick and has an area of 13 × 13mm ^{2}.

The band was wrapped around the upper-leg in such a way that it exerts no perceivable pressure, then was tightened in increments of two centimeters. After each increment the user bended his knees about 90 degree in a partial squat and the maximum of the signal was noted. This point was repeated after the signal with bent knees reached between 15% and 20% of the maximum (as given by sensor range).

The placement of the sensor on the muscle is performed according to international standards for EMG. The effect of the sensor displacement was also studied, resulting in the graphic of Figure 6.

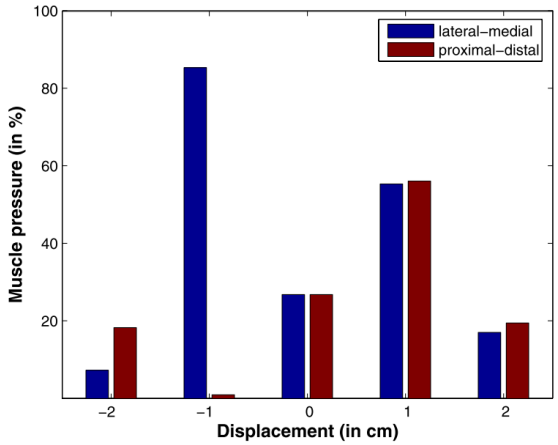

Figure 6: The effect of sensor displacement on signal quality (Lukowicz et al., 2009).

These measurements revealed that the optimal EMG placement spot does not correspond with the best placement for FSR sensors, although it does produce good signals, and that depending on the direction of sensor displacement even a 1 cm move from the original position can lead to a loss of signal. However, within a 4 cm × 4 cm square around the optimal position there are many points with good signal quality.

In the development of the project, they showed that under realistic assumptions it is possible to acquire good muscle activity signal with their approach, and information relevant for a range of pervasive applications can be extracted from this signal. In spite of these results, the muscles were not monitored while the subject was walking. In this dissertation this validation will occur also with the subject walking and the FSR signals will be compared with the EMG signals.

The group of Kreil et al. (2008) described the use of upper leg mounted FSR to analyse muscle activity during bicycling and demonstrated that FSRs can provide

information that is not accessible to motion sensors, like the gear in which a person is cycling or rather the amount of force applied to the pedals. Together with a sports clothing manufacturer (FALKE AG) they have developed special shorts for the integration of FSRs. A software calibration for the FSR sensors was made to linearise the data, by calculating the maxima and minima of the first peaks.

To measure the pressure changes of the leg muscles, four force sensors were integrated into running trousers, of size 46 mm x 46 mm. They were connected over an ADG708 multiplexer board and a current/voltage converter. The sensors were sampled at 25 Hz.

Figure 7 represents the sensor and clothes used, as well as the experiment setup.

(a) Trousers with integrated FSR sensors.

(b) Experiment Setup.

Figure 7: Kreil et al. (2008) Sensory System (Kreil et al., 2008).

Amft et al. (2006) compared the FSR sensors performance with fabric stretch sensors. Both of these sensors can be easily integrated into clothing. They used the above sensors to detect the contractions of arm muscles, and then compared the signals of each one. Figure 8 presents the experiments setup, where the larger white disks are the EMG electrodes, and Figure 9 shows the sensors hardware interfaces, consisting in a simple voltage divider for the FSR and a wheatstone bridge for the fabric stretch sensor. For this last sensor, the bandage is slightly stretched when the lower arm is relaxed and fixed using velcro.

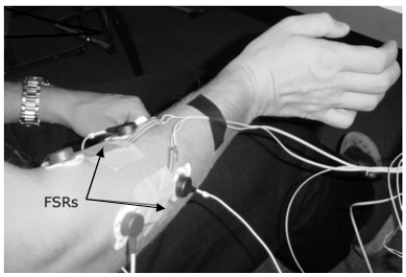

(a) Placement of FSRs on the lower arm.

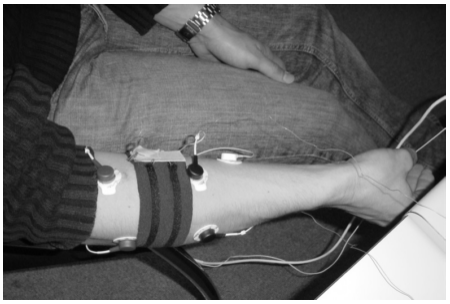

(b) Placement of fabric stretch sensor.

Figure 8: FSR and Fabric Stretch Sensor Setup Adapted (Amft et al., 2006).

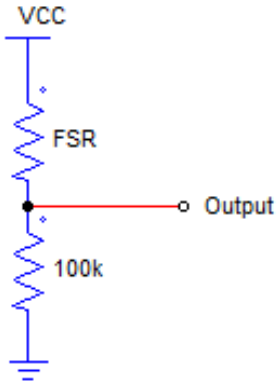

(a) FSR interface.

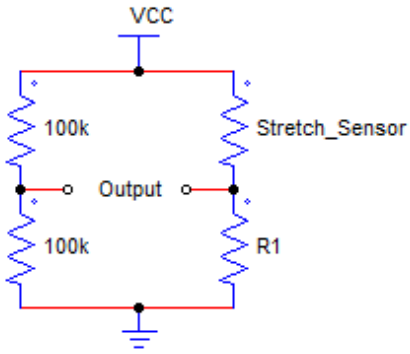

(b) Stretch Sensor interface.

Figure 9: FSR and Fabric Stretch Sensor Hardware Interface Adapted (Amft et al., 2006).

Figure 10 shows the results of the trials performed by these two sensors. The subjects performed four different actions, where Action 1 consisted in the upward movement of lower arm against resistance, Action 2 the outward bending of hand, Action 3 opening and closing hand (grasping motion) and Action 4 lifting of heavy object with right arm. The horizontal lines in the graphics highlight signal sections where the corresponding EMG amplitude exceeds a specific threshold value, indicating muscle activity and serving as a ground truth.

The results indicated that the proposed mechanical sensors provide alternative methods to detect muscle activities, and that such activities can be acquired from the various independent muscles at the lower arm. Furthermore, the results indicated that the FSR sensing concept is more applicable to the monitoring of individual muscles,

similar to EMG sensing, while the fabric stretch sensor cannot be used for monitoring individual muscles. In addition, the use of the fabric stretch sensor is limited due to the fact that the sensor exhibits a strong hysteresis.

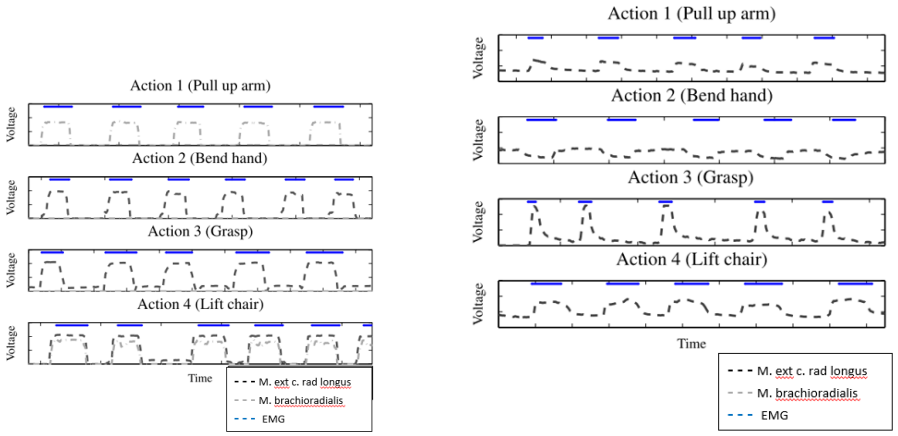

(a) Signals of the FSRs sensors. (b) Signals of the fabric stretch sensor.

Figure 10: FSR and Fabric Stretch Sensor Signals Adapted (Amft et al., 2006).

Ogris et al. (2007) presented an experiment that investigates the usefulness of muscle monitoring information from arm mounted FSR for activity recognition. Figure 11 illustrates the wearable system developed, with the FSR sensors integrated in an elastic sleeve on the forearm, considering the fact that palm and finger motions are driven by muscles in the forearm.

Figure 11: Contestant wearing the FSR sensor system, a MTx glove, and a mobile computer, that serves as a power source Adapted (Ogris et al., 2007).

Both the lower part of the forearm (right behind the wrist) and the upper part of the forearm (right under the elbow) are covered with a ring of four 46 x 46 mm FSRs. The sensors are integrated in a current/voltage converter, resulting in a linear relationship between resistance and output voltage with a much better dynamic range. Figure 12 demonstrates the signals of the upper four FSR channels. It was concluded that FSR based muscle monitoring is indeed useful for the recognition of activities involving hand actions and perform well for many individual gestures. This dissertation will study if it is possible to detect specific gait events by studying the signals acquired by the FSR.

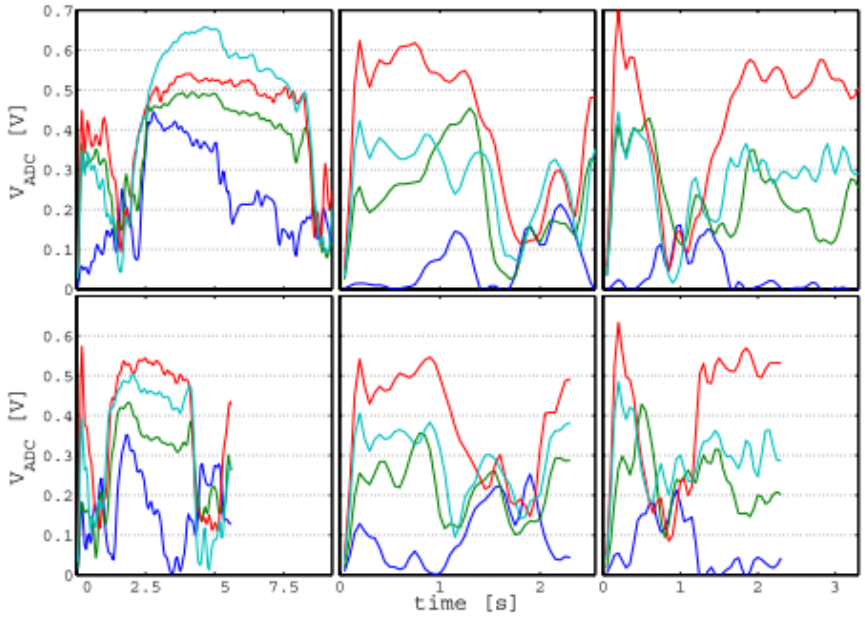

Figure 12: Signal samples for the upper 4 FSR channels, left column: 2 samples from class *drink*,middle: *open notebook*, right: *close notebook* (Ogris et al., 2007).

Another existing project, developed by Xiao and Menon (2014), consisted in proposing a novel system to detect different upper-extremities (forearm) postures in real-time, through the use of a lightweight and wearable forearm FSR strap. The FSR strap was designed to be placed on the proximal portion of the forearm and capture the activities of the main muscle groups with eight force input channels, as Figure 13 shows.

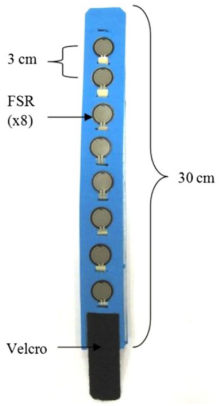

Figure 13: Interior view of FSR strap (Xiao and Menon, 2014).

Eight circular FSRs made by Interlink Electronics were inserted onto a strap made with FloTex foam; the FSR sensors were placed 3 cm apart from each other. The total length of the FSR strap was 30 cm. Velcro tapes were attached on both the interior and exterior end of the FSR strap to secure the strap onto user's forearm. The FSR strap was designed to be a simple device which can be worn without or with little assistance. The user does not require having muscle physiological knowledge in order to identify the location for the strap placement. He/she can simply wrap the FSR strap around the proximal portion of the forearm, and tight it up with Velcro. The amount of pressure needed to be applied to record *Force Myographic (FMG)* is mild, and with the flexibility of the FloTex foam, the FSR strap does not block blood circulation or constrain motion.

Voltage dividers were used for extracting the signals from the force sensor, as shown in Figure 14. The voltage divider circuit was powered by a 5 V voltage source of a *Data Acquisition (DAQ)* device made by National Instrument (NI USB 6210).

The obtained results confirmed that the FMG data captured from the FSR strap produced distinct patterns for the selected upper-extremities postures of the drinking task, but the muscles behaviour are not analysed individually, which is crucial for this dissertation.

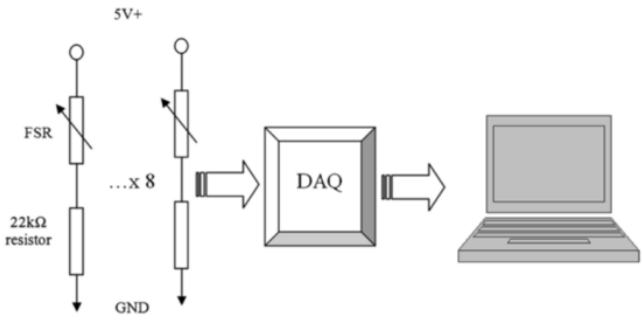

Figure 14: Xiao and Menon (2014) System diagram (Xiao and Menon, 2014).

2.1.2 *Capacitive Sensor*

Capacitive sensing is a useful technology for the measurement of multiple types of signals. The capacitance of the simplest capacitor, which consists of two non-contact metal plates, depends on the size of the metal plates and the distance between them. The relationship between capacitance and its relevant parameters can be used to measure distance, conductivity, pressure, etc., with various applications to pressure sensors, artificial skin and object detecting. This characteristic has another important application: sensing human movements (Zheng et al., 2013).

Meyer et al. (2006) developed a a pure textile, capacitive pressure sensor designed for integration into clothing to measure pressure on human body. Several textile sensors were developed with spatial resolution of 2x2 cm and an average error below 4 percent within the measurement range 0 to 10 N/cm^2. Applied on the upper arm the textile pressure sensor determines the deflection of the forearm between 0 and 135 degrees due to the muscle bending. The textile pressure sensor consists of a basic three-layer structure forming a capacitance with a pressure-sensing non-conducting dielectric as shown in Figure 15a. To achieve a spatial resolution an array of individually connected electrodes have been embroidered using silver coated yarn, as seen in Figure 15b.

To measure the capacitance of the textile electrodes, the capacitance to digital converter AD7745 from Analog Devices is used. All the measurement electronics are connected outside the textile.

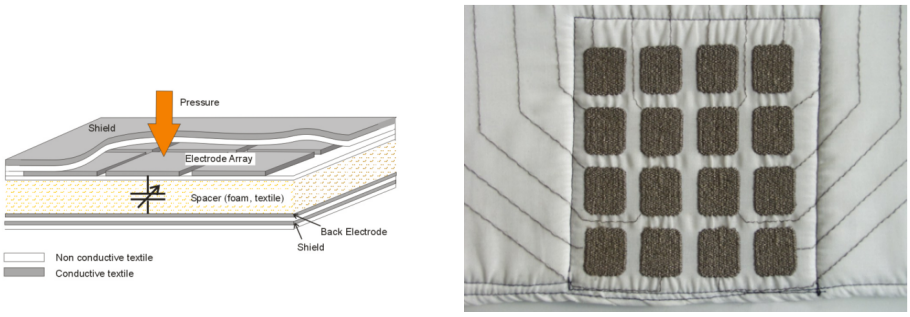

(a) Scheme of sensor with an array of textile capacitors and two shielding layers on both sides of the sensor.

(b) Textile Pressure Sensor with 16 sensing elements embroidered with conduc- tive yarn (shielding layers removed).

Figure 15: Meyer et al. (2006) Textile Pressure Sensor (Meyer et al., 2006).

The sensor has been used to detect the activity of the muscles of the upper arm. The sensor was fixed once on the *biceps* and *triceps* with an elastic band.

The capacitance-pressure has a hysteresis caused by the spacer. For that reason, to calculate the pressure at a given capacitance value, a model of the hysteresis is needed. For this purpose, the Preisach Model (Preisach, 1937) was applied. Figure 16 shows the results of the muscle activity monitoring.

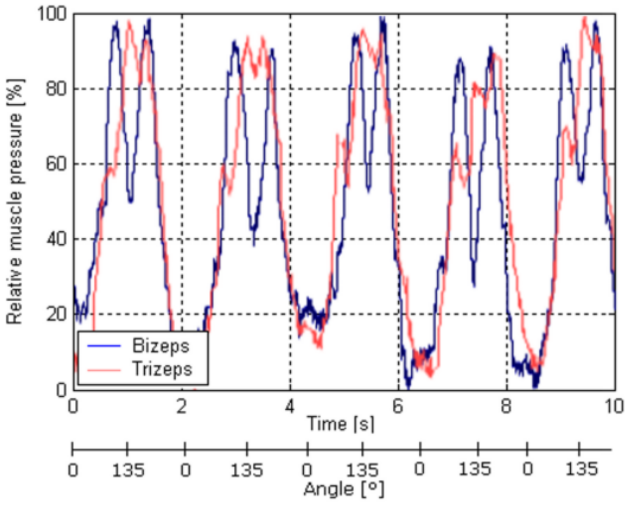

Figure 16: Muscle activity of *biceps* and *triceps* for periodically lifting a weight of 2 kg (Meyer et al., 2006).

These results showed that the textile pressure sensor can be used to measure pressure on human body, and that it was possible to detect muscle activity on the upper arm.

Zheng et al. (2013) presented an approach to sense human body capacitance and apply it to recognize lower limb locomotion modes. The proposed capacitive sensing system is made up of four parts: two sensing bands, a signal processing circuit, a gait event detection module and a computer to receive data streams. Figure 17 represents the developed system. A Velcro tie with circuits and batteries is fastened to the waist and shielding lines were used to reduce the noise.

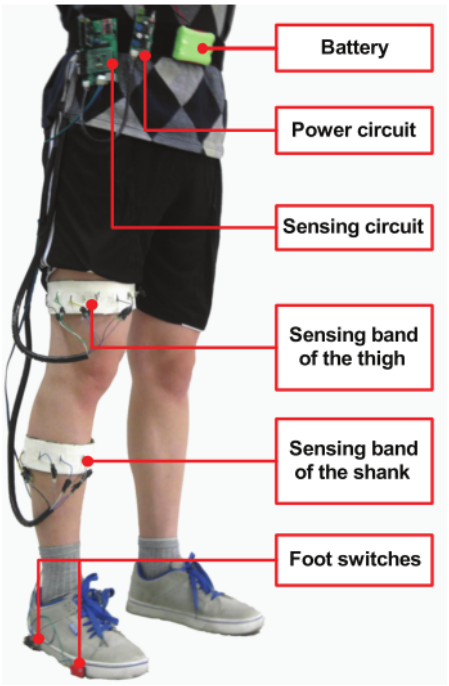

Figure 17: System Developed by Zheng et al. (2013) (Zheng et al., 2013).

Figure 18 shows the system architecture. The system consisted of the sensing circuit, the power circuit and the communication circuit. The sensing circuit was designed to process the capacitance signals from the sensing bands, including the oscillation module, the *Root Mean Square (RMS)*-converting circuit to convert the *Alternating Current (AC)* in *Direct Current (DC)* signal, and the control module. The circuit can process ten channels of signals at most.

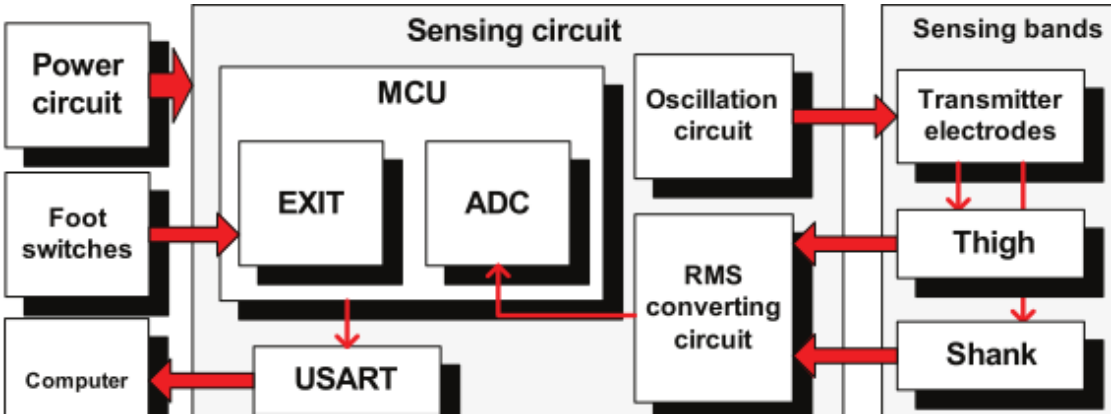

Figure 18: Zheng et al. (2013) System Architecture (Zheng et al., 2013).

Through this project development, it was concluded that as an alternative to EMG sensors and *Inertial Measurement Unit (IMU)* sensors, the capacitance sensing method can be further improved through hardware design and more thorough experiments.

Rekimoto (2001) introduced the GestureWrist, which is a wristwatch-type input device that recognizes human hand gestures by capacitively measuring wrist-shape changes and also measuring forearm movements. Figure 19a shows a schematic of the GestureWrist prototype.

Capacitive sensing is used for measuring the arm shape by placing both the transmitter and the receiver electrodes on a wristband, and for measuring finger positions by attaching electrodes on the inside of clothes. This principle is demonstrated in Figure 19b.

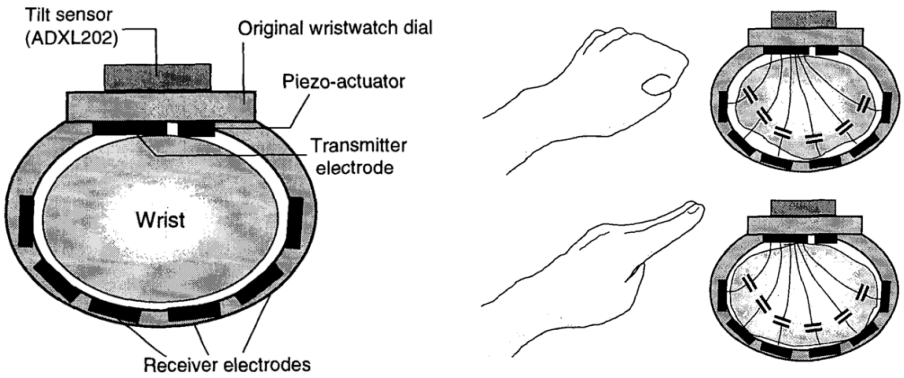

(a) Gesturewrist: A Wristband-type input device.

(b) Sensing arm-shape change based on capacitive sensing.

Figure 19: GestureWrist (Rekimoto, 2001).

2.1.3 *Other Sensors*

Jung et al. (2015) proposed a method to recognize the muscular activities. In order to detect the swelling of muscles in a reliable and convenient way, *pressure-based MMG (pMMG)* is introduced, based on air-pressure sensors and air-bladders. The muscular activity was detected by measuring the change of the air pressure in an air-bladder contacting the interested muscle(s). Since the change of the air pressure can be more robustly measured compared with the change of electric signals appeared on the skin, the proposed sensing method is useful for mobile devices due to its great *Signal to Noise Ratio (SNR)* and fast response time. Figure 20 shows an example of a schematic plot of an unit of an air-pressure sensor and an air-bladder.

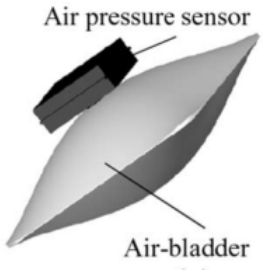

Figure 20: Unit of an air-pressure sensor and an air-bladder (Jung et al., 2015).

An air-bladder is made of *Polyvinyl Chloride (PVC)* films, the size of which is 35 mm × 40 mm. In the middle of the rectangular, a tube plug with the inner diameter of 3 mm was installed for connecting an air-pressure sensor. The outer diameter of a nipple of the air-pressure sensor is slightly larger than 3 mm, so that a sensor unit is completely closed and sealed. For durability, a rigid cover was installed in the sensory band.

A data acquisition board, NI-9205 and WLS-9163 of National Instruments Co., was used to measure the air pressure signals and the sampling frequency was set to 1 kHz. Six sensor units were enclosed in the sensory band. Figure 21 demonstrates the sensory band and its schematic.

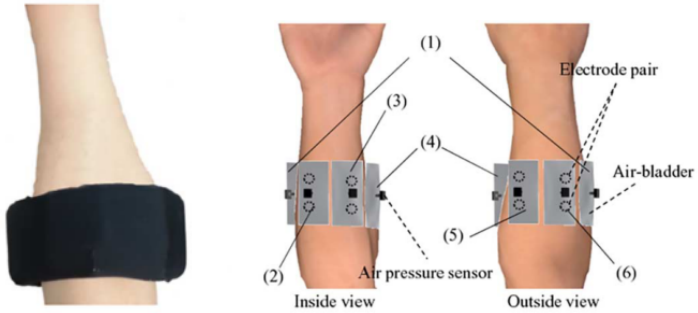

(a) Fabricated sensory band. (b) Location of air-bladders and electrodes.

Figure 21: Jung et al. (2015) Sensory band (Jung et al., 2015).

The pMMG signals were compared to the EMG signal, by measuring the magnitude of the *Maximum Voluntary Contraction (MVC)*, and with the IMU signal, measuring the relative angle of the wrist joint. The proposed system was able to measure the muscular force in advance to the change of the wrist angle, because the muscle contraction (which can be measured by the pMMG sensor) happens in prior to the motion of the wrist (which is measured by the IMU sensor). The pMMG signal also showed a better performance than the EMG signal, since the raw EMG signal showed a strong presence of noise and in order to filter it, the processed signal became slightly delayed compared to the proposed pMMG.

It can be concluded that the proposed pMMG system could detect the muscle activities, by measuring the pressure change in the air-bladder, which was induced by the swelling of muscles during voluntary contractions.

Kyoungchul Kong and Doyoung Jeon (2005) proposed a tendon-driven exoskeletal power assistive device to reduce some problems of the existing exoskeletal power assistive equipment. A *Muscle Fiber Expansion (MFE)* signal was used to control this device in order to compensate for the delay time of motors and perform an easy assistance by sensing the user's action in advance. The MFE signal has the characteristics that the signal is ahead of action and in proportion to joint torque. Figure 22 represents the tendon-driven exoskeletal power assistive device and caster walker.

Figure 22: Tendon-driven exoskeletal power assistive device and caster walker (Kyoungchul Kong and Doyoung Jeon, 2005).

The MFE sensor uses an air pressure plate and low priced pneumatic sensor. The MFE sensor was attached inside of thigh braces and is easy and simple to use compared to EMG sensors, which are directly attached at the exact points of muscle before the use of an *Exoskeletal Power Assistive Device (EPAD)*. In addition, this sensor is practical due to the use of a cheap pneumatic sensor when compared to a muscle hardness sensor which uses a load cell. Figure 23 demonstrates the principle of measuring of this sensor.

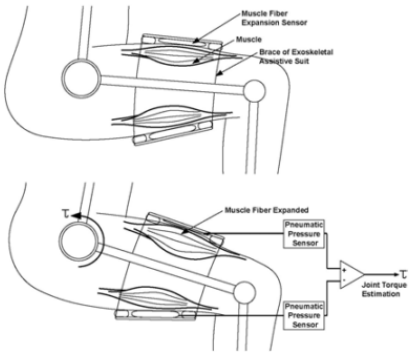

Figure 23: Principle of measuring the MFE signal (Kyoungchul Kong and Doyoung Jeon, 2005).

A comparison was made between the MFE and EMG signals. The MFE sensor presented very uniform value and less noise, though both signals are in proportion to the joint torque, as Figure 24 shows.

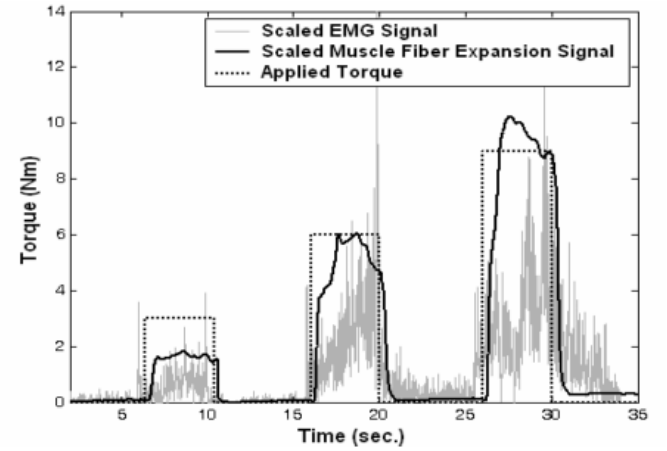

Figure 24: Comparison of the EMG signal and MFE signal (Kyoungchul Kong and Doyoung Jeon, 2005).

Wang et al. (2014) explored *Graphene Woven Fabrics (GWFs)* for highly sensitive sensing. A flexible and wearable strain sensor was assembled by adhering the GWFs on polymer and medical tape composite film. The signals of any weak motions, including breathing, phonation, expression changes, blink, and pulse, can be detected. In order to mould around human skin well to ensure the response of real signals, a good adhesive medical tape with *polydimethylsiloxane (PDMS)* glue, which is a flexible, bio-compatible, shape controllable material, upside as the substrate was used. As a new kind of electronic skin, it was made up with graphene woven fabrics, PDMS, and medical tape. Figure 25 shows the different positions where the tape was attached.

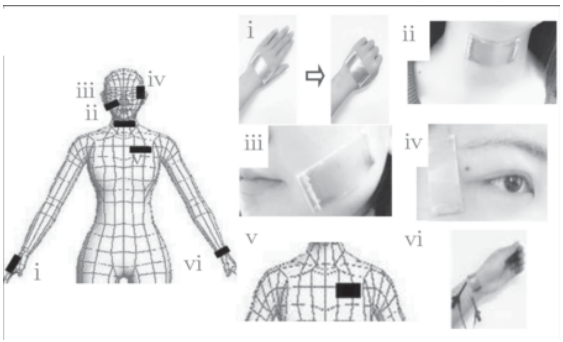

Figure 25: Photo images of GWFs- PDMS-tape at various positions (Wang et al., 2014).

After testing the sensor in several trials, it exhibited the following features: ultra-light, relatively good sensitivity, high reversibility, superior physical robustness, easy fabrication, ease to follow human skin deformation, without irritation, and so on. As a consequence of the piezoresistive effect of graphene woven fabrics, the sensors were used as electronic skin covering human body to detect body motions. The signals of GWFs resistance change depend on deformation strain which is formed by the motions. The stronger the motion is, the larger the strain is, and the easier the motion signals can be recorded.

2.1.4 *Sensors Comparison*

From these previous works presented, several conclusions can be drawn. There are many types of sensors able to detect muscle activity, as Table 1 demonstrates, although the FSR sensors have the advantage of being easily acquired in the market, can monitor individual muscles and can be easily integrated in clothes due to their flexibility, and also don't require complex electronics in order to integrate them and read their output signal. It is advised for their sensing area to be as bigger as possible to avoid errors due to their possible displacements. The FSR must also be covered in elastic tissue, so that they can detect the pressure made by the muscle stiffness, and require a simple hardware interface such as a voltage divider.

Table 1: Sensors Features

Sensors	Expensive	Flexible	Ease to find in Market	Must be Manufactured	Can Monitor Individual Muscles
FSR	No	Yes	Yes	No	Yes
Capacitive	Yes	Yes	No	No	Yes
Stretch Sensor	No	Yes	Yes	No	No
Air pressure	/	No	No	Yes	Yes
Graphene Woven Fabrics	/	Yes	No	Yes	Yes
Muscle Fiber Expansion	/	No	No	Yes	No

This dissertation will provide a way to monitor several muscles at the same time and calibrate the sensors signals through software methods, in order to make the system adaptable for every different individual. The output data will also be validated by comparing them with the EMG signals, by comparing them through their signal plots and through the calculus of several metrics. The system will be able to monitor any muscle, not being restricted to any of them. It will also be studied if the FSR sensors provide enough information to detect and recognize specific gait events, and the influence of several muscles in the human gait.

2.2 HUMAN MOTION RECOGNITION

This section main focus is to study existing methods of recognizing human motion.

Jung et al. (2015) used air pressure sensors and recognized six hand gestures, as shown in Figure 26, though fuzzy logic: the flexion and extension of the wrist [(a) and (b) in the figure]; the flexion and extension of the fingers [(c) and (d)]; and the radial and ulnar deviation of the wrist [(e) and (f)]. These hand gestures are anatomically related to different muscle groups, as in Table 2, and thus theoretically they should be able to be observed by the proposed sensor units located on the characteristic muscle groups.

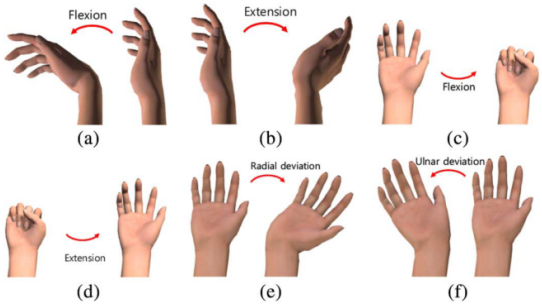

Figure 26: Activities to be recognized. (a) and (b) Flexion and extension of the wrist. (c) and (d) Flexion and extension of the fingers. (e) and (f) Radial and ulnar deviation of the wrist (Jung et al., 2015).

The normalized peak values during the six hand motions were studied, in order to understand the importance of each muscle activation in each gesture.

Table 2: Location of Muscles and Roles.

Location	Muscle	Role
(1)	*Flexor carpi ulnaris*	Flexion and ulnar deviation of the wrist
(2)	*Flexor digitorum*	Flexion of the fingers
(3)	*Flexor carpi radials*	Flexion and radial deviation of the wrist
(4)	*Extensor carpi radialis*	Extension and radial deviation of the wrist
(5)	*Extensor digitorum*	Extension of the fingers
(6)	*Extensor carpi ulnaris*	Extension and ulnar deviation of the wrist

The membership functions of the proposed fuzzy recognition algorithm are the functions of the pressures measured by the air pressure sensors.

The location of the muscles and the change of the cross- sectional area are all different for each person. For this reason, an auto-calibration process is necessary. In the experiments of this project, every subject was asked to squeeze as much as possible, so that the muscles were maximally contracted. During the execution, the level of MVC was measured for each muscle for normalizing sensor signals. The auto-calibration process greatly reduced uncertainty in the scaling factors for each trial and improved the success rate of the gesture recognition.

When the sum of the air pressure measurements is larger than a threshold, all the measurement values from six air pressure sensors are normalized by the largest value output among them. Otherwise, all the measurement values are set to 0. By this normalization, the measurement of the sensor unit is converted to the ratio of the air pressure, which is ranged from 0 to 1.

Each air bladder has three membership functions: 1) a low phase membership function; 2) a middle phase membership function; and 3) a high phase membership function. The output of each function represents the likelihood of the air pressure measurement, i.e., pMMG, to be in each phase, i.e., low, middle, and high.

The rule base of the fuzzy logic is designed as in Table 3, based on the membership functions. The rule base was mainly determined by the role of muscles for each gesture and the air bladders corresponding to the muscles.

Table 3: Rule Base Of Fuzzy Logic.

Gesture	(1)	(2)	(3)	(4)	(5)	(6)
Wrist flexion	Mid	High	High	Low	Mid	Mid
Wrist extension	Mid	Low	Low	Mid	High	Low
Finger flexion	Mid	High	Mid	Low	N/A	Low
Finger extension	Low	Low	Low	Low	High	None
Radial deviation	Mid	Low	Low	High	N/A	Mid
Ulnar deviation	Low	High	Low	Low	Mid	Low

The performance of the proposed gesture recognition system was verified with multiple subjects by checking the success rate of gesture recognition.

Beil et al. (2015) presented a force-based control approach, which allows the generation of motion pattern based on interaction force pattern between the exoskeleton and the human body. Instead of using movement information as a control scheme, the interaction forces acting between exoskeleton and user's body are used

as input of the controller to make predictions of the user's motion. In general the prediction of the users knee motion is performed by measuring the summed forces contributing to the knee joints with the FSR sensors and control the position of the linear actuator in a way which result in reducing the interaction forces.

The force signals processed by an Arduino are smoothed, multiplied with gains taking account the size of the sensor interface as well as the position of the sensor and summed up to define a criterion for the effective interaction force.

Figure 27 illustrates the functioning of the control approach. The filtered and computed control variable is derivated once and filtered again to sustain a smoothed input for the derivative term of a *Proportional–Integral–Derivative (PID)* controller. The *Finite Impulse Response (FIR)*-filter used for the smoothing of the derivative values is a weighted moving average filter of 9^{th} order. Beneath the derivative term the control variable is also integrated to receive the integral term of the PID controller. The proportional term is provided by the weighted interaction force itself.

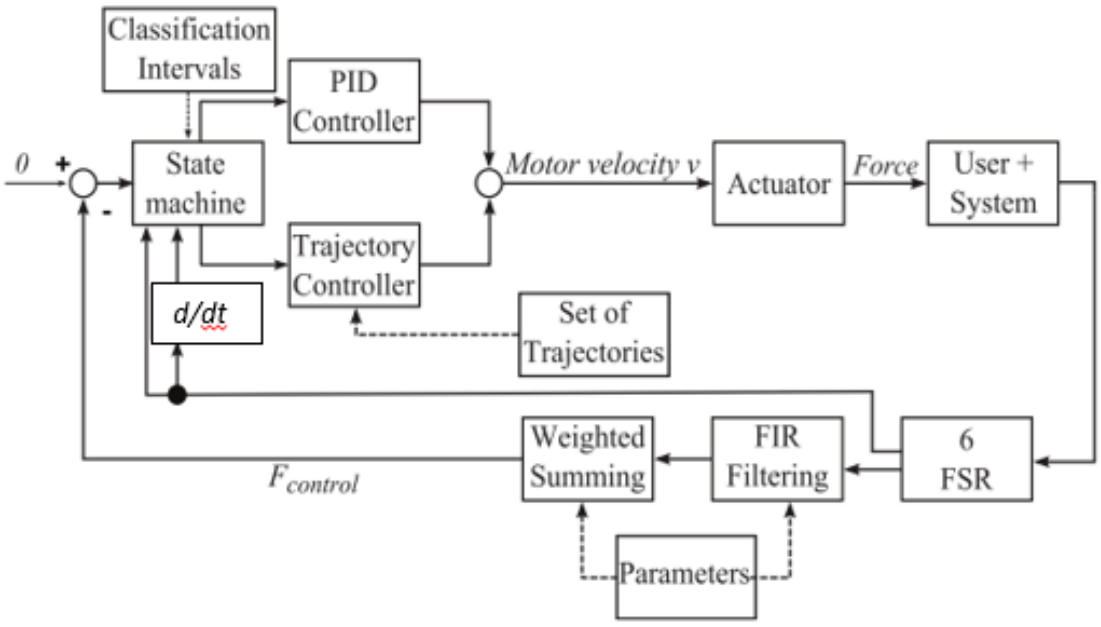

Figure 27: Block diagram of the proposed control approach (Beil et al., 2015).

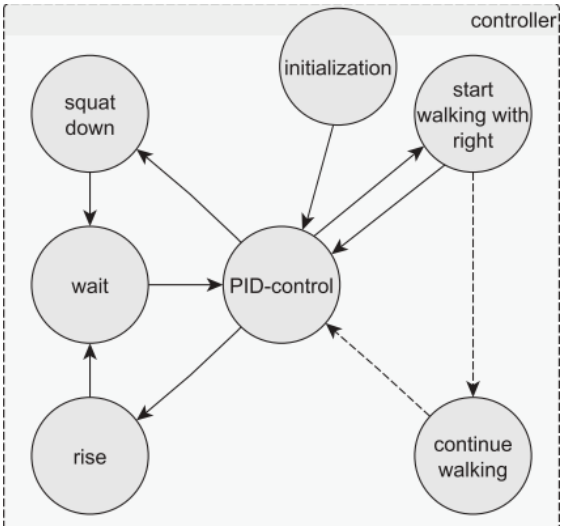

Figure 28: Finite state machine to select the predicted user movement Equation (Beil et al., 2015).

Before reaching the controller a finite state machine (Figure 28) compares the control signal to trigger intervals to select the mode of operation. If no predefined motion is detected the PID controller is used and the exoskeleton shadows the leg movement of the user without exerting forces on it. Force signals corresponding to predefined motions will result in a switch in the state machine to a mode where the motor controller is commanded by predefined trajectories. In this mode the exoskeleton guides the user's leg.

This study concluded that it is possible to recognize specific human motions though the pressure applied is between the user and the exoskeleton.

Kreil et al. (2008) recognized the gear in which a person is cycling. To recognize the amount of used strength while cycling, which corresponds to the different gears, the raw sensor data was calibrated, using the 5 cycles in the highest gear. Then the data is segmented into steps with the segmentation algorithm. On these steps 2 features on the 2 sensors on the back of the thigh were calculated. Feature 1 is the difference between maximum peak and minimum peak (peak amplitude), the second is the absolute value of the average slope between two minimum peaks. Both results are median filtered over the last 5 cycles. To recognize the different gears, these two features were presented to a tree based C4.5 classifier and the *k-Nearest-Neighbor (kNN)* classifier, implemented in the YALE library. Because of the small number of data sets,a cross validation scheme was used, training the classifiers with 5 data sets and testing the classification model on the remaining data set. The results showed that

when using the two classifiers to detect every single gear, the overall detection rate is between 20 and 50 per cent. Also, by comparing the classification results of the grouped classes between calibrated and non calibrated data it can be concluded that linear calibration can return a benefit in the data evaluation. In terms of recognition rates that can be achieved on the specific example, there is clearly still considerable room for improvement.

Ogris et al. (2007) focused on recognizing 16 different hand gestures. For comparison, three classifiers have been tested. The tree based C4.5 classifier and the in- stance based kNN were used in a sliding window approach: In a time window of fixed size, a set of features was computed using the raw sensor data. Then the sliding window is moved by an offset which determines the overlap with the last window. Mean and variance were used as features, with window size 30 and step size 15. After that, a majority decision was applied to the raw classification results. This yields a filtered decision for the particular gesture and constitutes the final result of the frame based classification. The YALE implementation of these classifiers was used.

In addition to this frame based approach a *Hidden Markov Models (HMM)* based classifier was tested as well. For each manipulative gesture in the experiment a separate HMM was trained. During testing a single gesture was aligned with the most likely model. The HMM implementation was used in the Bayes Net Toolbox for Matlab for the experiments. The classification results for the three classifiers are summarized in Table 4.

Table 4: Ogris et al. (2007) Classification results in % (Ogris et al., 2007).

Classifier	Acc	Gyr	Fsr	Acc+Gyr	Fsr+Acc	Fsr+Gyr
HMM	83	72	73	91	84	81
C4.5	76	57	62	82	79	68
kNN	81	65	76	90	86	84

The recognition was far from perfect for all combinations of sensors and all classifiers. This was to be expected, as the gesture set was chosen to test the limits of the recognition rather than to be fully recognizable.

Zheng et al. (2013) proposed a human gait recognition method. Gait events of *Foot Contact (FC)* and *Foot Off (FO)* could be detected. According to these two gait events, four phases were defined: prior to FC, after FC, prior to FO and after FO (they are marked as Pre-FC, Post-FC, Pre-FO and Post-FO, respectively).

The *Linear Discriminant Analysis (LDA)* classifier was employed for locomotion mode recognition, and five *Time-Domain (TD)* features were chosen for candidate features, according to the following expressions: $f1 = avg(X), f2 = max(X), f3 = min(X), f4 = rms(X), f5 = std(X)$, where X is the data matrix of the analysis window, $avg(X)$ is the mean value of X, $std(X)$ is the standard deviation of X and $rms(X)$ is the root mean square of X, As a result, a 50-dimension feature value set was used for classifier training and testing.

As mentioned above, five basic TD features were chosen as the candidates to form the feature set. All the combinations of the features(31 combinations in total) were calculated and the results are shown in Figure 29.

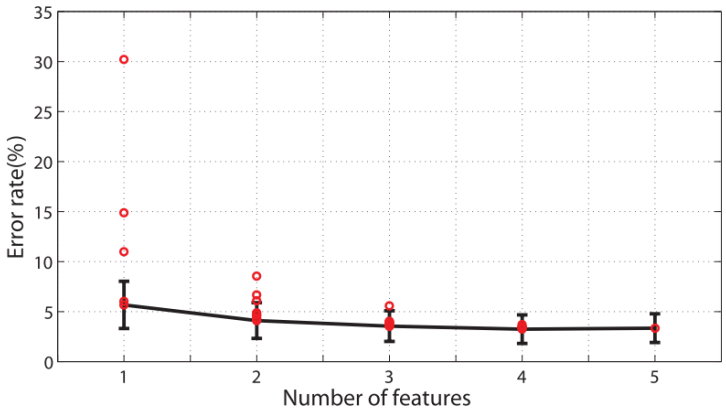

Figure 29: Classification errors of different combinations and numbers of features (Zheng et al., 2013).

For the single features, $avg(X)$ and $rms(X)$ performed much better than the others with the average error rate being 6.0% and 5.7% respectively. While $std(X)$ performed the worst with the error rate of 30.2%. The red dots represent the average classification errors of all the subjects in a specific number of features. The lowest error rate among the combinations is denoted as the black line. The error bar is the standard deviations of the subjects. The results are obtained by the LDA classifier with a 200-ms window size.

The classification performance was compared with signals from the thigh, the shank and both (Figure 30). For all the four events, classification using signals from both the shank and the thigh achieved the best performance.

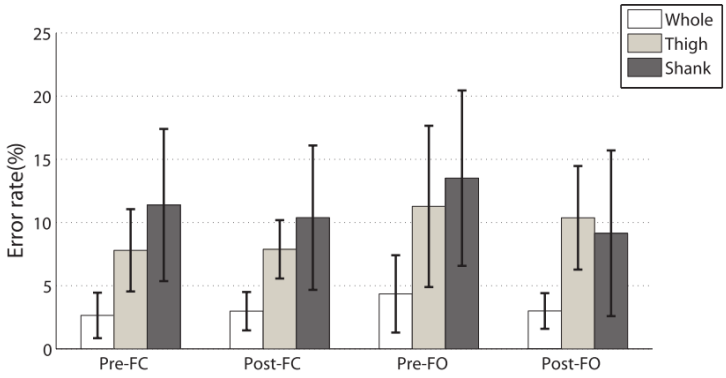

Figure 30: Classification errors of different combinations of signal channels (Zheng et al., 2013).

Xiao and Menon (2014) developed a non-kernel based *Extreme Learning Machine (ELM)* classifier with sigmoid based function that was implemented for real-time classification due to its fast learning characteristics, in order to distinguish different upper-extremities postures. The input data was the FSR data positioned in a strap. The non-kernel based ELM has an output function, as Equation 1 shows.

$$f(x) = h(x)\beta \tag{1}$$

$h(x)$ is the hidden-layer output corresponding to the input samples from the sensors ($\boldsymbol{x}\ \epsilon\Re^8$), and β is the output weight vector between the hidden layer and the output layer. For multiclass classification, the predicted class label is the index number of the output node that has the highest value.

A total of six classes were included, and each class corresponding to one distinct posture for the drinking task as shown in Figure 31.

The postures were associated with the movement, such as rising the forearm (elbow flexion), grasping or releasing the cup (fingers flexion/extension), and repositioning the cup to mouth (wrist pronation). The average real-time testing accuracy was 92.33% with a standard deviation of 3.19%. From the results, it was concluded that the ELM was able to accurately extract the pattern in real-time for the drinking task.

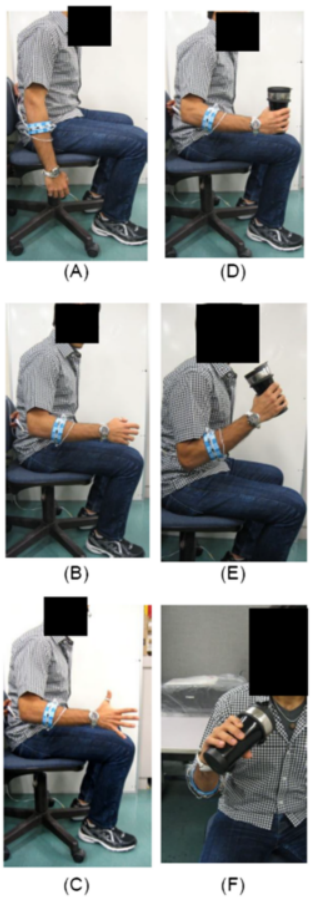

Figure 31: Classes definition for drinking task postures (Xiao and Menon, 2014).

From these studies it can be concluded that there are many existing methods for recognizing human motion, from fuzzy-logic control, to a state machine, or a machine learning algorithm could be implemented, due to its high rate of success.

This dissertation will recognize specific gait events. Since there is an order to them, the algorithm used will be a finite state machine, which input is the FSR data.

3

PROBLEM ANALYSIS

This chapter targets the definition of this dissertation the main theoretical concepts, and present the *MuscLab* system and its influence in the *SmartOs* system.

3.1 THEORETICAL CONCEPTS

Before the system development, certain areas needed to be addressed and studied, such as the muscles dynamics and the human gait analysis.

3.1.1 *Muscle Contraction*

In muscle contraction, there are three different types: 1) isometric; 2) concentric; and 3) eccentric contractions. The characteristic of the isometric contraction is that there is no change in the muscle length. An example of the isometric contraction is maintaining a posture or holding an object. Although the muscles generate forces to maintain the posture or to hold the object against the gravity, the lengths of the muscles do not change because the joint motion is stationary.

On the other hand, in the concentric contraction, the muscular force is generated while the length of the muscle is shortened. For example, when a human lifts up an object, the associated muscles generate muscular forces and their lengths are shortened.

In the eccentric contraction, the length of the muscle lengthens while generating muscular forces. The simplest example of an eccentric contraction is lowering a heavy object in a biceps curl.

Gestures or motions occur if the lengths of the muscles change. Therefore, the eccentric and concentric contractions of muscles result in or are resulted from motions. (Jung et al., 2015).

Some motions also required contractions of both antagonist muscles at the same time. While one muscle contracts in a concentric way the other one has an eccentric contraction.

3.1.2 *Human Gait*

The human gait analysis addresses the systematic study of the human walking, which involves the monitoring of spatiotemporal, kinematic and kinetic gait data. This analysis has potential to be applied as an assessment tool of the gait pathologies and the locomotion performance of the athletes, as well as a strategy to contribute to real-time information for the assisted-as-needed control, demanded on neurorehabilitation.

A gait cycle can be defined as a time period between the foot initial contact with the floor until the moment that the same event occurs with the same foot. This cycle can be divided in two phases: stance and swing. The stance phase corresponds to the time period in which the foot is pressed on the floor, and the swing phase corresponds to the time period in which the foot is in the air, as Figure 32 shows (Figueiredo et al., 2017).

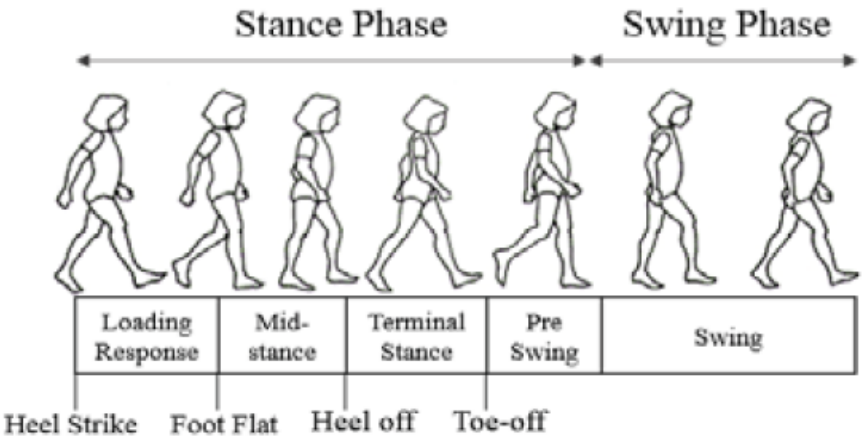

Figure 32: Gait Cycle (Figueiredo et al., 2017).

As represented in Figure 32, the stance phase contains several events, beginning with the heel strike, which marks the beginning of the stance phase when the heel is pressed against the floor, followed by the foot flat event, when the foot is all pressed

against the floor, heel off is when the heel is lifted, and finally the toe-off event, when the foot is in the air, starting the swing phase.

3.2 MUSCLAB

MuscLab is the proposed wearable system that is integrated in the *SmartOs* project, with the purpose of achieving the goals presented in Chapter 1. This system consists in a device attached to the user and contains FSR positioned in several specific muscles. These sensors allow the user's muscular activity monitoring and recognizes the toe-off gait event. This data can be analysed in real-time or in offline mode. This device allows the monitoring of 7 different muscles at the same time, with a frequency sample of 100 Hz.

Figure 33 represents the *MuscLab* system overview. This system consists in a device that collects data from the FSR sensors positioned in the muscles. The sensors data is acquired through a voltage divider and a low-pass filter before being processed in the MCU, which calibrates the signals and recognizes the gait event. The final data is then sent to a GUI, or saved in a memory card, or sent to the *SmartOs* MCU.

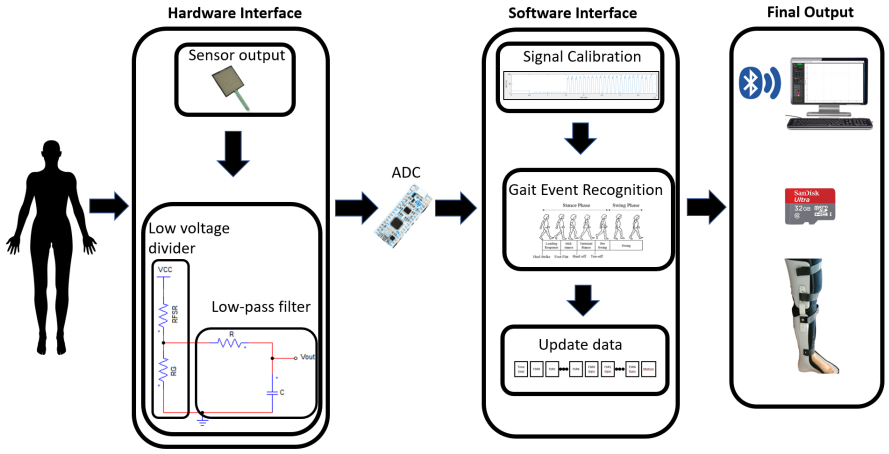

Figure 33: System Overview.

The device is supplied by a battery, which supplies the MCU. The microcontroller chosen was the *STM32F303K8* due to its plenty available resources. This MCU is responsible for acquiring and processing data from the sensors which are connected to the microcontroller *Analog-to-Digital Converter (ADC)*, and supplying and communicating with the remaining hardware components. The bluetooth module

allows the wireless connection between the device and the desktop application, and is connected by serial port. The MCU is also connected through *Serial Peripheral Interface (SPI)* with a memory card SD shield to allow data storage in a memory card. The force sensor used is the FSR because of its easy integration in clothes and its easy acquittance in the market. Figure 34 summarizes how the main components used are related.

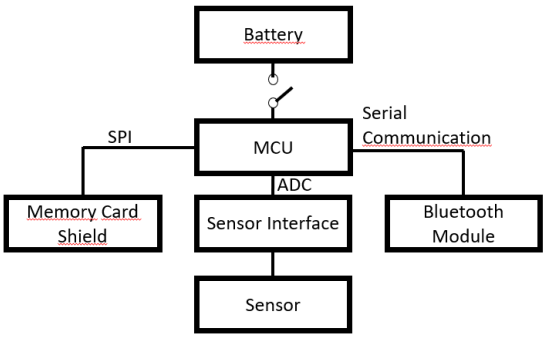

Figure 34: Modules Overview.

Despite the MCU led, which turns on when the device is powered on, the device contains 3 more leds (red, green and yellow), allowing the system to alert the user of its respective status. Table 5 represents the led code for each status.

Table 5: System Status.

Status	Leds Activated		
	Red	Yellow	Green
Low Battery	X		
Trial Running			X
Calibration Running		X	X
SD Card Error		X	
Idle			

LOW BATTERY: Battery charge is low. The user must turn off the device and recharge its battery as soon as possible. If battery charge is less than 5 %, the system will enter in a shut down mode, in which the red led will blink and the system will save the data in the memory card if a trial in offline mode is running before blocking every function, "freezing" the MCU.

TRIAL RUNNING: A trial is running at the moment.

CALIBRATION RUNNING: In the beginning of each trial, the first 5 seconds are used to calibrate the system.

SD CARD ERROR: This error can happen when there is a problem initializing or writing in the memory card.

IDLE: No trial is running.

3.2.1 *SmartOs*

SmartOs includes a smart, stand-alone active lower limb orthosis -AAFO - synergistically interconnected with a wearable motion lab to treat the spastic gait via a smart rehabilitation upon a pharmacotherapy (injection of botulinum toxin). To achieve this goal, *SmartOs* incorporates a smart hierarchical control architecture bioinspired on the principles and organization of the human motion-control system (three-level architecture). This architecture generates assistive commands according to the user's motion state and disability level (monitored by the wearable motion lab) both de-codified by adaptive learning technologies. These technologies were designed to timely recognize and predict the intended motion, to detect incipient falls and the user's impaired level, to segment gait cycle, and to automatically tailor the dynamic behaviour of the human-orthosis interface.

Wearable motion lab aims the real-time monitoring of the patient's motor status (i.e., the user's motor ability, and spasticity level) and the human-orthosis interaction. This wearable motion lab includes ergonomic, stand-alone, wearable sensory systems, such as: (i) *GaitShoe* to measure force-ground contacts for the gait segmentation; (ii) *InertialLAB*, formed by different miniaturized sensors to monitor the biomechanical motion of limbs and joints; (iii) *MuscLAB* to objectively monitor muscle activation/ weakness instead the use EMG-signals prone to the user's sweating and electrodes shift; (iv) *VibrotactileLab*, a non-invasive technique to monitor the spasticity. Additionally, *SmartOs* explores wearable biofeedback mechanisms (e.g., time-discrete feedback provided for a vibrotactile systems - Waistband) to encourage the user's active participation and to seamless the bidirectional interaction between the user and AAFO.

4

HARDWARE INTERFACES

To ensure the system ergonomics are still reliable, its hardware must be as simple and reduced as possible.

4.1 MAIN COMPONENTS

In this section, the several components used are presented, as well as their main features. Table 6 sums the main components used and their prices per unit available in the market. These components were chosen in order to ensure the system ergonomics by making its dimensions as small as possible.

Table 6: Main Components.

Component	Quantity	Price (unit)
STM32F303K8	1	10.12$
Hacker LiPoBattery 7.4 V/900 mAh	1	11.95 euros
FSR	7	11.95 $
Memory Card Shield SD	1	4.80 euros
HC-06 Bluetooth Module	1	6.90 euros

4.1.1 *MCU*

The development board used, presented in Figure 35, is a *STM32 Nucleo-32* development board, with a *STM32F303K8* MCU.

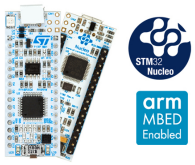

Figure 35: STM32 Nucleo-32 (STMicroelectronics, 2018a).

This development board provides an affordable and flexible way for users to try out new concepts and build prototypes with the *STM32* microcontroller, choosing from various combinations of performance, power consumption and features.The Arduino Nano connectivity makes it easy to expand the functionality of the *STM32 Nucleo* open development platform with a choice of specialized shields.The *STM32 Nucleo-32* board does not require any separate probe as it integrates the *ST-LINK/V2-1* debugger/programmer and it comes with the *STM32* comprehensive software HAL library, together with various packaged software examples, as well as direct access to the *Advanced RISC Machine (ARM)* embed Enabled on-line resources (STMicroelectronics, 2018a). Table 7 sums this board main features.

Table 7: STM32 Nucleo-32 Characteristics (STMicroelectronics, 2018a).

Parameter	Value
Micro controller	*STM32F303K8*
Architecture	ARM
Voltage Supply (USB)	5 V
Voltage Supply (External)	3,3 V; 5 V; 7 - 12 V
Memory flash	32 KB
Data Memory	32 bit
SRAM	16 KB
Clock Speed	48 MHz
Timers	11
Analog Pins	9
Pins	32
PCB size	18,54 x 50,29 mm

This board stands out due to its small dimensions and its resources, such as its high clock speed and available peripherals. Although it can be supplied by a 3,3 V, 5 V or

7 to 12 V, in order to gain access to the MCU debugger, it can only be supplied from 7 to 12 V.

4.1.2 *Battery*

In order to run the system, a voltage supply is needed to power up the MCU. The battery chosen was the Hacker LiPoBattery 7.4 V / 900 mAh, demonstrated in Figure 36.

Figure 36: Hacker LiPoBattery 7.4 V / 900 mAh (BotnRoll, 2018).

This battery was selected mainly because of its small dimensions, voltage output and current capacity, as shown in Table 8, fulfilling the MCU needs.

Table 8: Hacker LiPoBattery 7.4 V / 900mAh Features. (BotnRoll, 2018).

Parameter	Value
Voltage	7.4 V
Balancer plug-in	TP
Technology	LiPo
Connector system	EC3
Dimensions	30 x 68 x 13 mm
Weight	55 g
Number of cells	2
Capacity	900 mAh
Electrical load	25 C

4.1.3 *Sensor*

The sensor to be used will be the FSR, available in Figure 37. As already explained in Chapter 2, this sensor was chosen due to its flexibility and it is easy to integrate in clothes, allowing the system to become wearable. This sensor changes its resistance value as the force applied in the sensing area changes. To minimize interferences due

to possible displacements of the sensor the sensing area must be as big as possible. Table 9 list the FSR main features.

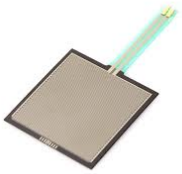

Figure 37: Force Sensing Resistor (MakerBright, 2018).

Table 9: FSR Main Features (MakerBright, 2018).

Parameter	Value
Dimensions	1.72″
Sensing Area	1.56″ × 1.56″
Force Sensitivity Range	0.2 - 20 N
Stand-Off Resistance	>1 MΩ
Weight	1.2 g

4.1.4 *Memory Card Shield SD*

A memory card shield, represented in Figure 38, was used in order to allow to save data in a memory card by a microcontroller. Table 10 sums the module main features. The communication protocol used is SPI instead of *Secure Digital Input Output (SDIO)*, since the SPI protocol can be interrupted while the software code is running and the SDIO can not.

Figure 38: Memory Card Shield SD. (good, 2018).

Table 10: Memory Card Shield SD (good, 2018).

Parameter	Value
Voltage Supply	3.3 V
Dimensions	3.5 cm x 2.2 cm
Interface	SPI and SDIO

4.1.5 *Bluetooth Module*

The bluetooth module was the "HC-06 Bluetooth Serial Module". This module communicates with the MCU through serial communication, capable of baudrates of 115200 bps maximum and a wireless range of 10 m (Botnroll, 2018). This module establishes the communication between the device and the desktop application. Figure 39 shows the bluetooth module used and Table 11 its characteristics.

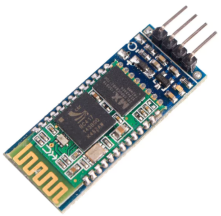

Figure 39: HC-06 Bluetooth Serial Module. (GearBest, 2018).

Table 11: HC-06 Main Features (Botnroll, 2018).

Parameter	Value
Voltage Supply	5 V
Logic Voltage	3.3 V
Interface	Serial Communication (RX TX pins)
Maximum Baudrate	115200 bps

4.2 BATTERY INTERFACE

Figure 40 shows the voltage supply interface. Right after the battery there is a switch that allows the user to turn on and off the voltage supply. Then a schottky

diode is inserted right after the switch to protect the microcontroller against negative voltages, in case the user switches the battery terminals. It was chosen a schottky diode instead of a regular one due to its reduced commutation time and low forward voltage drop, to dissipate the minimum energy possible from the battery. In parallel there is a ceramic capacitor, functioning as a decoupling capacitor, with the purpose of helping stabilizing the battery output voltage. In parallel there are two resistors in which the voltage divider will provide the battery voltage status with the MCU ADC reference.

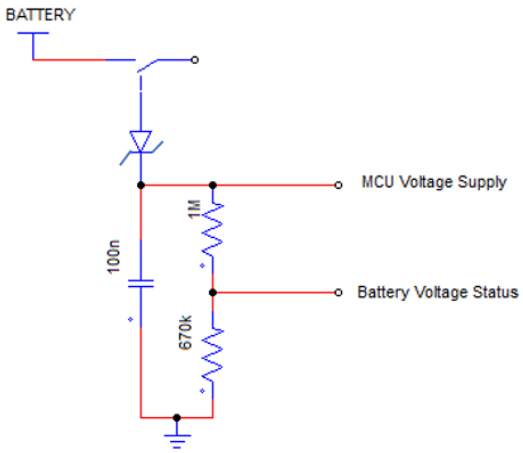

Figure 40: Voltage Supply Interface.

4.3 SENSORS INTERFACE

In order to obtain a voltage drop from the FSR sensor value into the MCU, a hardware interface is needed to connect these two. Figure 41 shows a simple voltage divider. RFSR represents the FSR resistance value and RG the hardware gain, which impedance is 160 Ω. This resistance value is low to avoid signal offset and high gains that may turn the signals non linear. This interface is powered by the MCU.

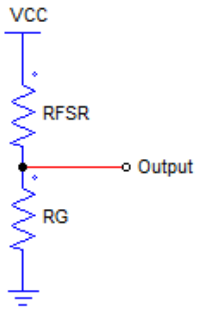

Figure 41: Voltage Divider.

The output obtained is the voltage drop in RG. Equation 2 represents the output of this configuration.

$$Output = VCC \times (\frac{RG}{RFSR + RG}) \tag{2}$$

Beside the voltage divider, a low-pass filter (Figure 42) was implemented to ensure that the signal acquired from the FSR does not contain aliasing.

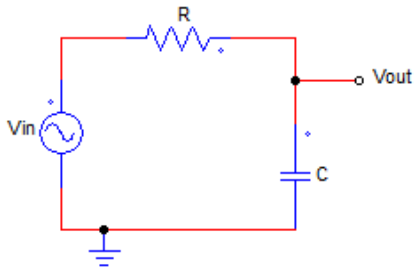

Figure 42: Low-pass Filter.

The time constant and cutoff frequency (Hz) can be calculated by Equation 3 and 4 respectively.

$$\tau = RC \tag{3}$$

$$fc = \frac{1}{2\pi\tau} = \frac{1}{2\pi RC} \tag{4}$$

The resistor R used was 150 kΩ and the capacitor C 100 nF, which leads to a time constant of 15 ms and a cutoff frequency of 10.6 Hz. These values were chosen in order

to not cause delays in the signal and to ensure lower frequencies are not filtered. The *Discrete Fourier Transformation (DFT)* of a FSR signal acquired when the subject was walking was measured, concluding that the signal frequency is around 0.5 Hz, so the filter time constant and cutoff frequency fit.

By combining these two circuits, it is obtained the final sensor interface, demonstrated in Figure 43. This interface proves that the FSR sensors require very simple electronics, which can be designed in reduced dimensions and containing few cheap components, instead of the hardware required by the EMG signal acquisition.

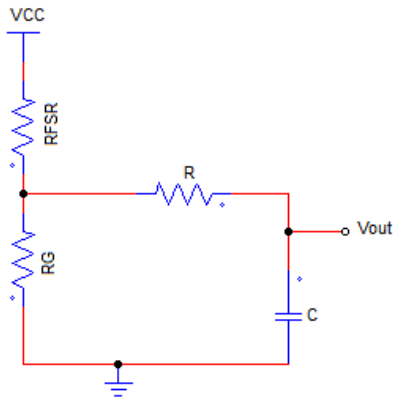

Figure 43: Sensor Interface.

In this interface it was also analysed that it should contain a buffer between the voltage divider and the low-pass filter to isolate these two configurations. This process guarantees that the cutoff frequency calculated is not influenced by the voltage divider.

4.4 PCB DESIGN AND DEVELOPMENT

The device PCB was designed in the PADS software. In Figure 44 it can be found the PCB schematic and board file. To ensure the device ergonomics, the hardware was designed so that the PCB would have reduced dimensions.

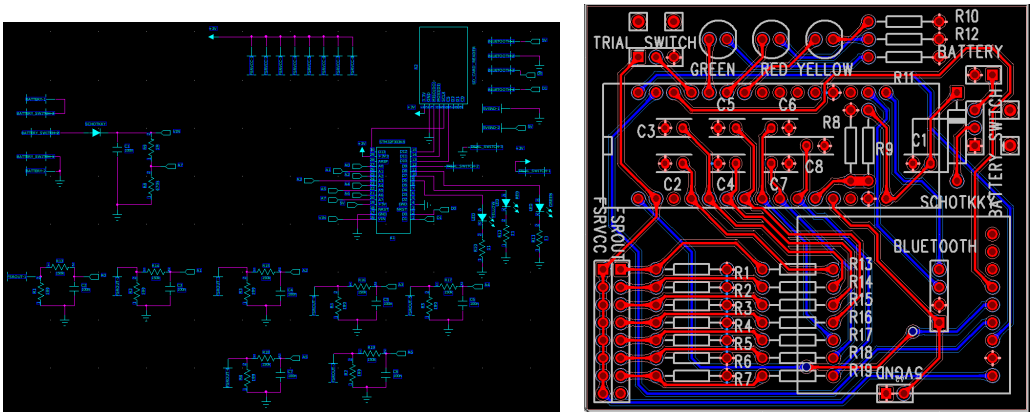

(a) PCB Schematic. (b) PCB Board.

Figure 44: PCB Design.

The board dimensions are 63.5 x 58.42 mm, which are acceptable to be integrated in a wearable system. Figure 45 shows the final prototype.

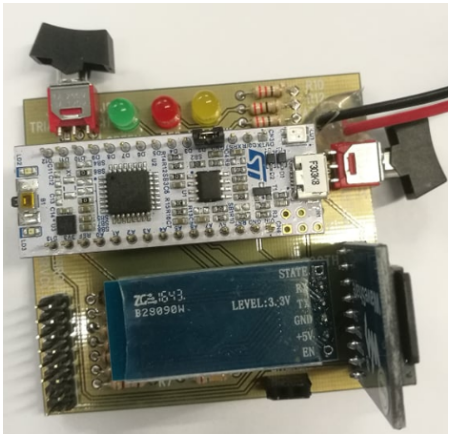

Figure 45: *MuscLab* Development Board.

4.5 DEVICE CASE

To ensure the user's comfort, a case to store the device and attach it to the user's limb by the aid of a strap was developed. This process required first the case design in the tool *SolidWorks*, which is a *Computer Aided Design (CAD)* 3D software, and then printed in a 3D printer. Figure 46 shows the *SolidWorks* case design.

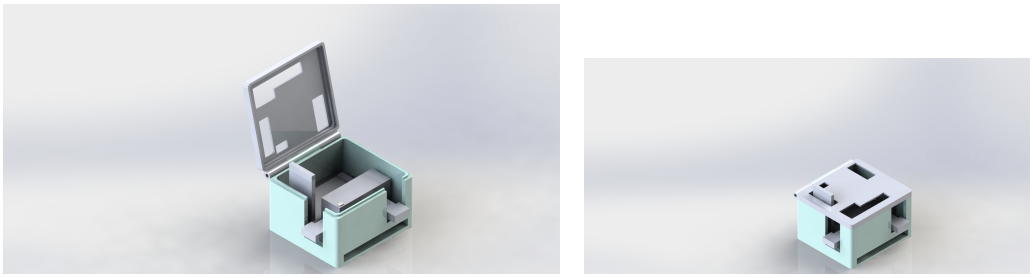

(a) Opened Case. (b) Closed Case.

Figure 46: SolidWorks Case Design.

The case cover contains several holes in top of the PCB leds to make them visible to the user so that he can understand the system status, in top of the memory card module pins, to allow the user to insert and withdraw the memory card at will, and also in top of the FSR pins, to insert/withdraw them also at ease without needing to open the case. This aspect improves the device ergonomics.

5

SOFTWARE INTERFACES

The software design and development was divided in two stages, such as programming the MCU (low level) and the GUI (high level).

5.1 MICROCONTROLLER (LOW-LEVEL)

The MCU was programmed in the Keil uVision5 *Integrated Development Environment (IDE)*, with the aid of the STM32CubeMX firmware. This firmware is part of STMicroelectronics STMCube original initiative to make developers' lives easier by reducing development effort, time and cost. By selecting and configuring the MCU peripherals, it generates the code in C, using the HAL library, and create a Keil project with the code generated (STMicroelectronics, 2018c). The code is organized in several modules, as Figure 47 shows. Each module is responsible for a specific task, in order to allow the code to be more robust and practical.

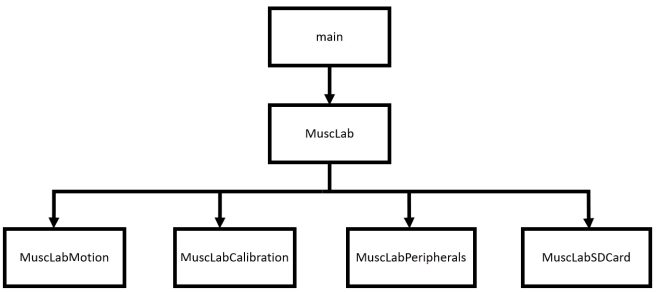

Figure 47: Microcontroller Code Modules.

The main module contains the program main state machine, which calls the functions implemented in the *MuscLab* module. This module is also responsible for connecting the remaining modules, such as the *MuscLab Motion*, in which the

gait event recognition functions are implemented, the *MuscLab Calibration*, where the signal calibration functions are implemented, the *MuscLabPeripherals*, responsible for the MCU peripherals functions and the *MuscLabSDCard* which uses the *FatFs* library in order to connect with the memory card. The timer 1 is configured to activate its *Interrupt Service Routine (ISR)* function, responsible to activate the flag which allows the program to read the sensors output in periods of 10 ms, to achieve a sample frequency of 100 Hz. The timer 2 is responsible for allowing the program to read the battery voltage. Since this variable has a more gradual evolution (the system requires low energy), its sampling period is 30 seconds. Figure 48 represents a flowchart of the main state machine algorithm.

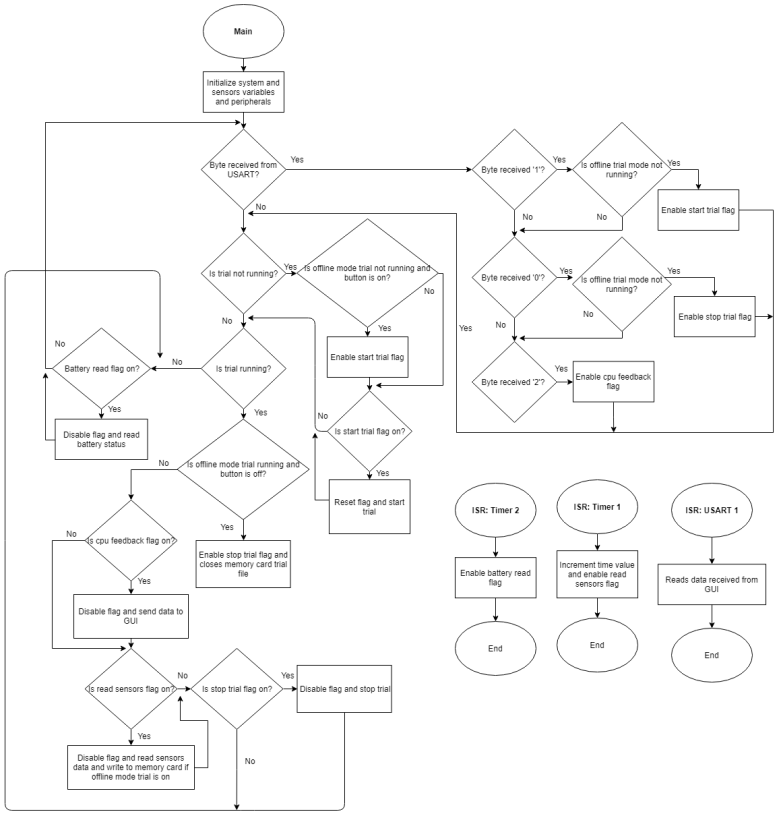

Figure 48: Main State Machine Flowchart.

Figure 49 represents a flowchart of the *MuscLab* module functions. When starting a trial, the system resets its values and checks if the trial will run in offline or online mode. If it starts in offline mode the program will first check if the memory card is correctly inserted and ready to be written, otherwise an error will occur. If all

conditions allow the system to start a trial, the timer responsible for reading the FSR data will be activated. This timer is turned off at the end of the respective trial.

Although in offline mode the data is printed in the memory card every time the sensors output are sampled, in online mode the data is only saved and updated and is only sent to the desktop application when it is received an acknowledge byte from the GUI, allowing a synchronism between the device and the desktop application.

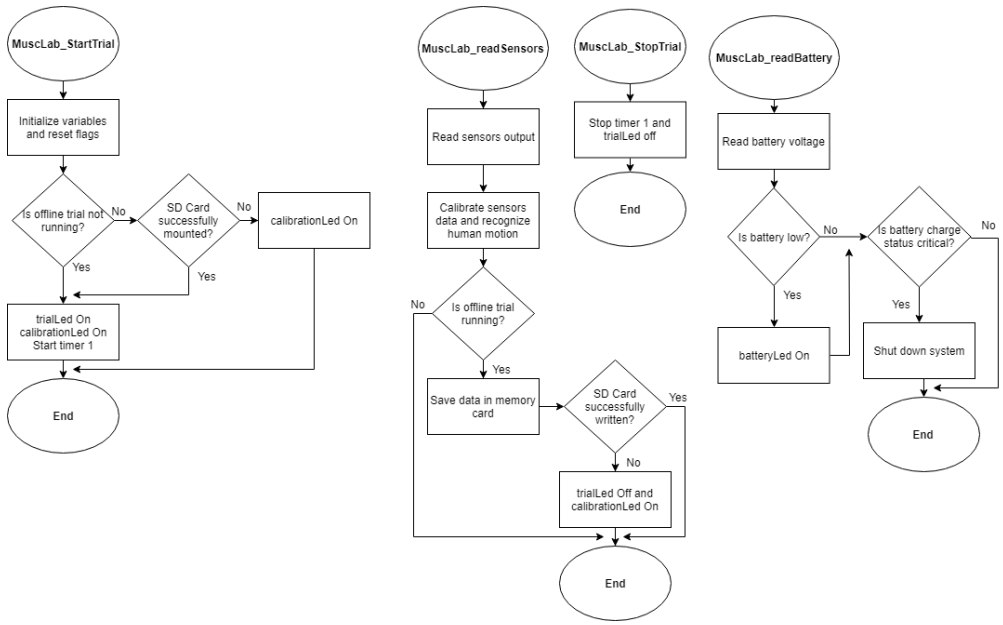

Figure 49: MuscLab Functions Flowchart.

When the battery charge is checked, the system will analyse if it is low. If so the system warns the user by turning on the low battery led. If the battery charge enters a critic state, the MCU will immediately turn off its peripherals and block every function, becoming not operable. It was studied the value read from the MCU ADC for each input voltage, and for each of that value associate with a percentage from 0 to 100, representing the battery charge level percentage. With those values, a linear regression was made, with the aid of the *MatLab* tool, represented in Figure 50, resulting in Equation 5.

$$battery = 2.58867 \times input - 478.054 \tag{5}$$

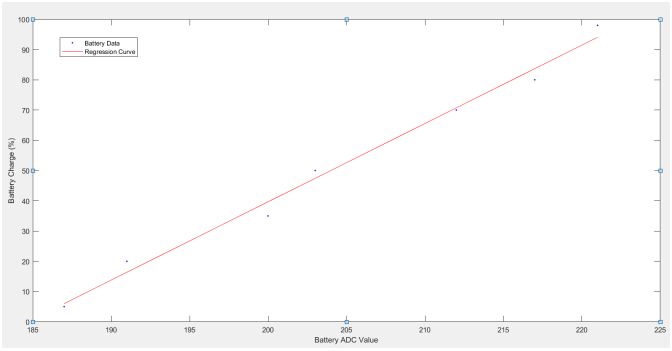

Figure 50: Battery Charge Equation.

5.1.1 *MuscLabCalibration*

This module is responsible for the FSR signals calibration. This calibration consists in three different stages, as represented in Figure 51.

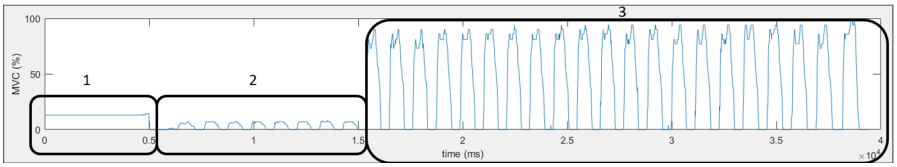

Figure 51: Signal Calibration Stages.

The first stage will be acquiring data while the muscle is relaxed in the beginning of each trial in a period of 5 seconds, and with that it will be possible to remove the signal offset by calculating its mean value and subtract it to the sensor output signal. The second stage of the software calibration is the calculus of the sensors software gains while the subject is contracting the respective muscle. These gains are found by measuring the sensors maximum values and then the gains are applied in a way that the maximum values reach 100 when multiplied by them. These gains are updated in periods of 10 ms. The third stage is when these gains are already being applied and still being updated until the end of trial.

The flowchart presented in Figure 52 sums up the signal calibration algorithm.

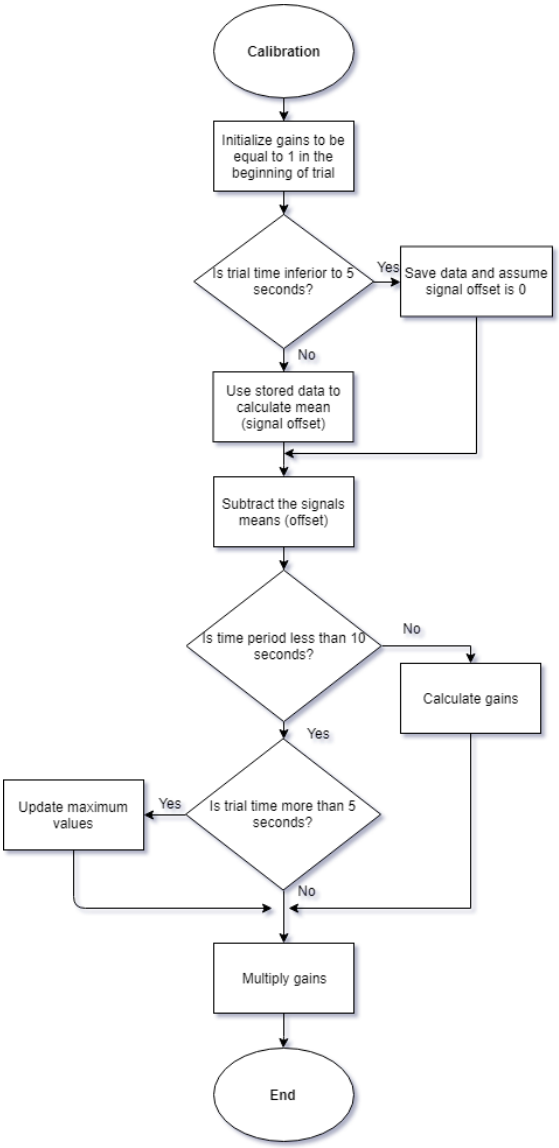

Figure 52: Signal Calibration Flowchart.

5.1.2 *MuscLabMotion*

In this module are the functions regarding the gait event detection and recognition. This algorithm was developed in order to detect and recognize the gait event toe-off, which ends the stance phase and initiates the swing phase. The muscles monitored in this algorithm are the *anterior tibialis* and the *gastrocnemius* muscles.

Figure 53 represents the algorithm flowchart. This algorithm first step is to make sure the gait event will only be detected and recognized if the current trial is past the offset calibration. If that is the case, the algorithm will analyse which is the current phase (stance or swing). If it is the swing phase, the program will analyse if the FSR value of each muscle is above the threshold values defined. If this condition is verified, it means that the subject is now in phase stance. Finally if the subject is already in phase stance and the FSR values are lower than the threshold values, it means that the user is currently in the toe-off gait event. This event is here detected and recognized and also from here begins the swing phase.

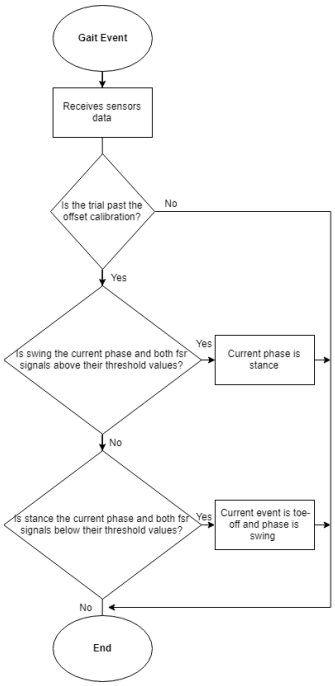

Figure 53: Gait Event Recognition Flowchart.

5.1.3 *Output*

The microcontroller output, which is sent to the GUI and saved in the memory card, is an array of bytes, which is represented in Figure 54. This array contains 16 bytes, in which the first byte corresponds to the time in milliseconds which that data was sampled, followed by the sensors output values. After the sensors outputs comes the sensors gains (result of the sensors software calibration that are updated in periods of 10 ms), and finally the last byte indicates the current gait event detected.

Figure 54: Output Array.

5.2 DESKTOP APPLICATION (HIGH LEVEL)

The GUI was developed in the QT Creator environment. Qt Creator is a cross platform IDE to create C++ and *Qt Modeling Language (QML)* applications for multiple desktop, embedded and mobile platforms.This IDE was chosen due to its simple and intuitive interface, features a code editor with syntax highlighting and auto-completion, drag-and-design UI creation, visual debugging & profiling tools and many other tools (Qt, 2018). The language used to program the desktop application was C++, since it is a highly portable language and is often the language of choice for multi-device, multi-platform app development, and is an object-oriented programming language and includes data abstraction and a modular code.

Figure 55 represents the GUI developed. This application can only be run in online mode. The device must be already powered on and no trial should be running in offline mode.

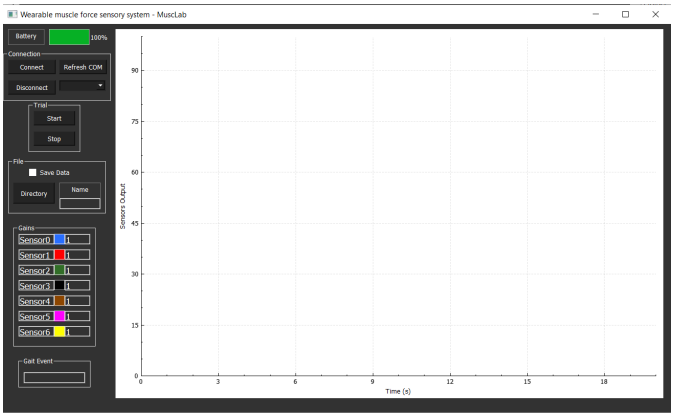

Figure 55: Desktop Application.

The buttons are all divided in group boxes, such as the connection to the device buttons, the start and stop trial command buttons and the file writing functions. The battery charge level can be analysed in the top left corner, showing its percentage. The sensors gains provided from the MCU software calibration are also available in this

application, below the file buttons box, and showing the plots respective colours. In the bottom left corner is displayed the current gait event detected, and finally, in the right side of the application it can be analysed the muscles signals plots.

With the flowchart presented in Figure 56, it is clearer to observe that the GUI main tasks are to establish the bluetooth communication with the device, by sending data such as the command to start or stop a trial or an acknowledge to receive further data. Another main task is to parse the data coming from the device and update the values displayed, to allow the user to study the sensors signals in plots and their gains and the current gait event detected, and write the data in a txt file if that option is enabled.

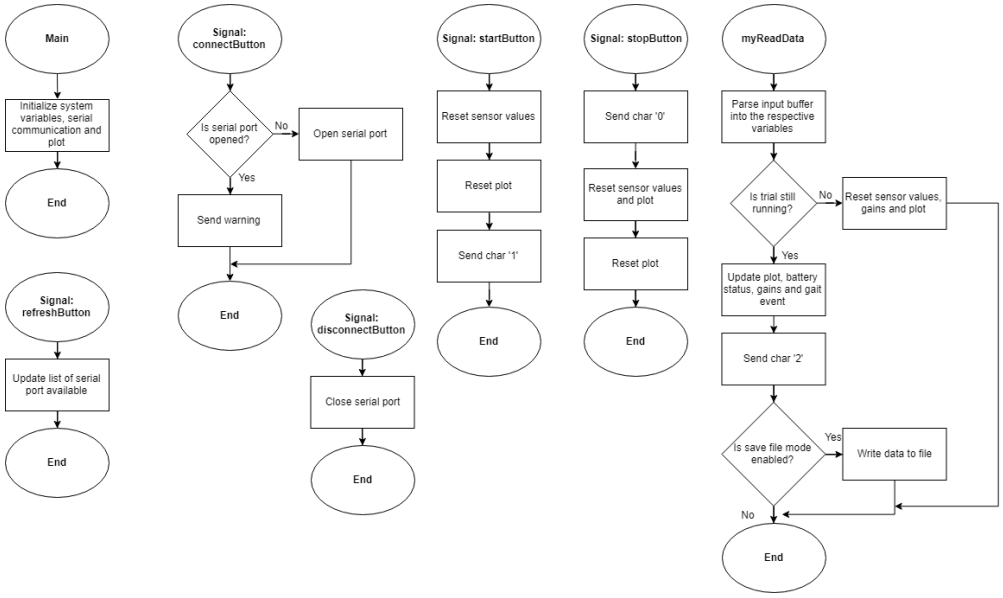

Figure 56: GUI Flowchart.

5.3 INTEGRATION IN THE SMARTOS SYSTEM

As it was explained in Chapter 3, this system is one of the subsystems integrating the *SmartOs* system. To integrate it in the *SmartOs*, the code implemented in the *MuscLab* MCU must be transferred to the *SmartOs* microcontroller. Figure 57 shows the *SmartOs* several modules that are integrated in it.

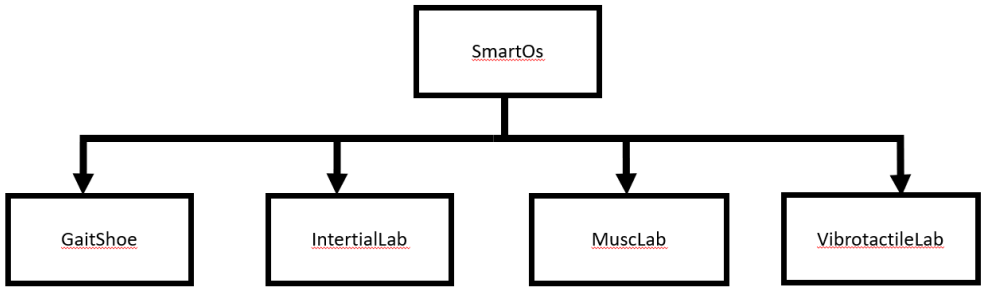

Figure 57: *SmartOs* Modules.

The development board where these modules are implemented is the *STM32F4DISCOVERY*, illustrated in Figure 58. From this board the data is acquired and processed and sent later to the system *Central Processing Unit (CPU)*, which is a *Raspberry Pi*.

Figure 58: *STM32F4DISCOVERY* (STMicroelectronics, 2018b)

This board contains the *STM32F407VG* MCU, and contains many resources, such as featuring 32-bit ARM Cortex, 1 Mbyte Flash memory and 192 Kbyte *Random Access Memory (RAM)*, and an oscillator frequency of 160 MHz maximum.

One advantage of integrating the *MuscLab* in this MCU is the fact that both microcontrollers are compatible, containing both ARM architecture, so the low level functions are similar. Another advantage is that both systems are programmed in modules, so that the integration becomes more practical. The *SmartOs* development board was already developed in order to acquire data from 7 analogic pins. To integrate the *MuscLab* code in this MCU, it was only needed to copy the timer 1 configuration in order to acquire data from the analogic pins in periods of 10 ms, and the functions responsible to process that data, such as the signals calibration functions and the gait event recognition functions. The functions responsible for sending data to

the GUI and saving it in a memory card were withdrawn, as well as the battery reading function, because the *SmartOs* modules purpose is to update the data acquired in each one of them, in order to send the the data to the system CPU.

The *MuscLab* board MCU is withdrawn, as well as the battery. The board is supplied by connecting the 3.3 V and GND pins to the *SmartOs* board, and the sensors output pins instead of being connected to the former MCU is connected to the *SmartOs* board analogic pins.

6

SYSTEM VALIDATION

In this chapter it will be presented two different validation trials, one corresponding to the FSR signal quality by comparing it to the EMG signal, studying regression models with the purpose of converting the FSR to EMG signal, and finally studying the gait detection algorithm accuracy in the trials already performed.

6.1 FSR EMG SIGNAL COMPARISON

This section consists in describing the trials protocols, such as which muscles will be monitored, the types of sensors to be used and their hardware interfaces , the trials procedure, and finally the results obtained.

These trials will be divided in two groups: static and dynamic. The static trials were performed in the CMEMS laboratory and the dynamic trials were performed in the *Laboratório de Biomecânica do Porto (LABIOMEP)*, located in the *Faculdade de Desporto da Universidade do Porto (FADEUP)* facilities, due to their available equipment and resources capable of providing better and more realistic results.

6.1.1 *Static Trials*

Three subjects participated in these trials, repeating each trial 3 times. The subjects studied had different gender, age (24.33 $\pm$ 2.31), weight (67 $\pm$ 8.89 Kg) and height (1.7 $\pm$ 0.07 m).

It was used two types of sensors in these trials, as Figure 59 shows, such as the electrodes to obtain EMG signals and the FSR sensors, to measure the muscular strength. In order to obtain these two signals as much synchronized as possible, the FSR sensors were placed in top of the electrodes, sharing the same muscle location.

(a) Electrodes (Olimex, 2018).

(b) FSR (MakerBright, 2018).

Figure 59: Sensors Used.

For the EMG signal acquisition 3 electrodes were used on the target muscle, one serving as reference (inserted on top of the knee) and the other two to obtain the voltage drop (located in the muscle belly). These electrodes are connected to a customized EMG signal acquisition board, as shown in Figure 60, developed in the laboratory. This board contains two potentiometers, one for calibrating the the signal gain and the other the signal offset. The PCB also contains seven stages, as Figure 61 shows, such as an instrumentation amplifier for potential acquisition, initial amplification (x50) and common mode rejection; a bandpass filter (20 Hz to 500 Hz) and a notch filter to attenuate the effect of the noise and the power network; an amplification stage to increase the resolution, allowing the signal to be readable without losing information; a full wave rectifier (depending of the state of the switch), for signal rectification; and finally, a voltage limiter for protection of the digital processing unit using the ADC reference. The output is connected to a microcontroller. This description shows how much more complex the EMG signal acquisition hardware is, comparing with the FSR sensors hardware interface designed in the *MuscLab* system.

Figure 60: EMG Signal Acquisition Board.

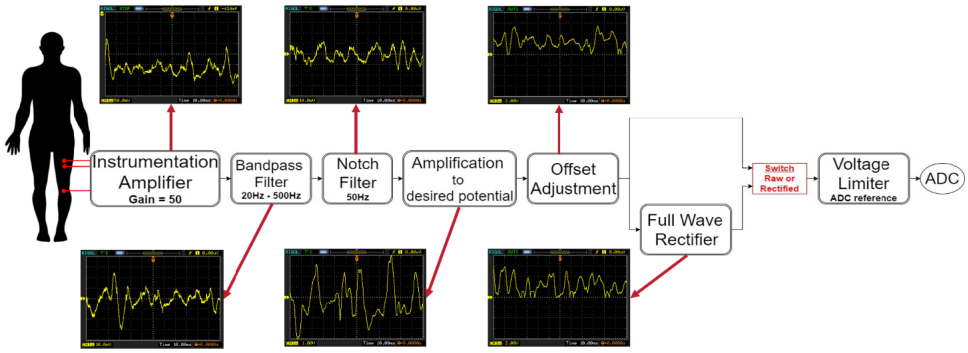

Figure 61: EMG Signal Acquisition PCB Stages.

To obtain the FSR signal, the FSR sensors were placed in top of the electrodes, perpendicular to the respective muscle belly, covered with an elastic band to ensure that the muscles activations apply pressure in the FSR sensors, as Figure 62 shows.

Figure 62: Sensors Setup.

For these trials it was used 4 PCBs, represented in Figure 63: 2 EMG signal acquisition boards, 1 responsible for converting 5 V to -5 V to supply the EMG signal acquisition boards and also for providing the same ground to all boards, and finally the system device PCB, where the MCU is located. The sensors final output are all connected in this last development board. For these trials both signals were acquired

with a sample frequency of 500 Hz. In the static trials it was used a development board without the low-pass filter allowing to use this sample frequency.

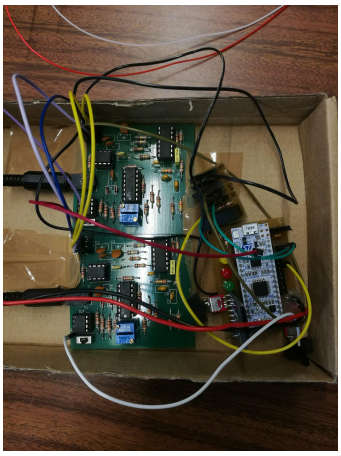

Figure 63: Trials PCBs.

To validate the leg muscle activity monitoring in the static trials, the motions to be performed were the ankle *plantarflexion* and *dorsiflexion* (Figure 64a) and the knee flexion and extension (Figure 64b).

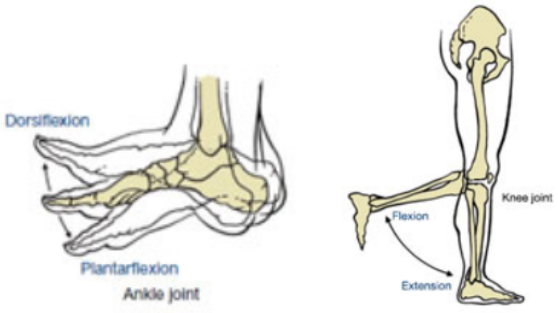

(a) Ankle *Dorsiflexion* and *Plantarflexion*.

(b) Knee Flexion and Extension.

Figure 64: Ankle and Knee Motions (AceFitness, 2018).

The muscles to be monitored regarding the ankle motions were the *anterior tibialis* and the *gastrocnemius*, illustrated in Figure 65 due to their influence in these specific movements (AceFitness, 2018).

(a) *Gastrocnemius*. (b) *Anterior Tibialis*.

Figure 65: Ankle Plantarflexors and Dorsiflexors (AceFitness, 2018).

For the knee movement, the muscle to be monitored was the the *vastus lateralis* (Figure 66), which is responsible for the knee extension (AceFitness, 2018).

The leg motions to be studied were performed and repeated 10 times in each trial. The trials are repeated 3 times.

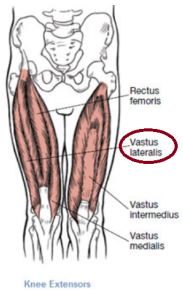

Figure 66: *Vastus Lateralis*.

The metrics calculated were the Pearson Correlation, the delay between the EMG and FSR signals, and their *Root Mean Square Error (RMSE)* percentage. These metrics were calculated by using the *MatLab* functions. Figure 67 shows an example of the signals output. The top plot is the raw signal acquisition and the bottom plot displays the data filtered, by using a butterworth second order filter, with a cutoff frequency of 1.6 Hz. This filter was applied due to the EMG raw signal containing lots of noise.

Since this filter induces a delay to the raw signal, this filter was applied in both signals in order to obtain a better comparison between them. The calibration period in the beginning of each trial was also withdrawn, in order to calculate the desired metrics.

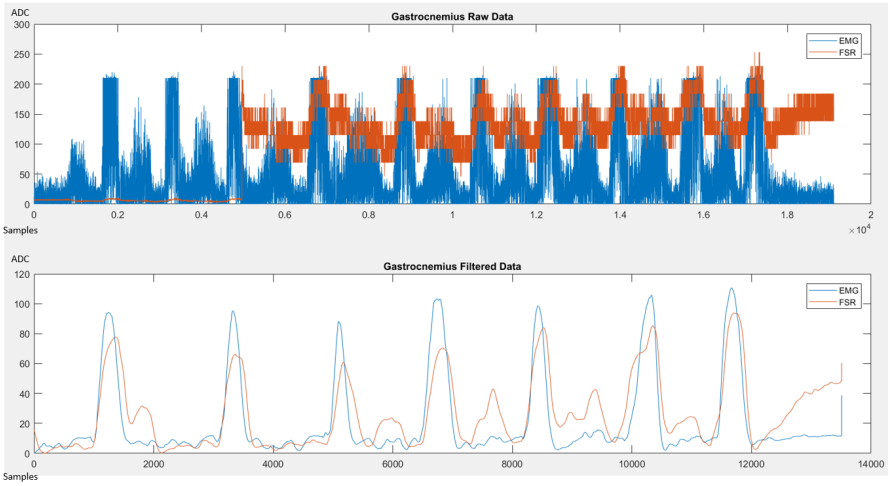

Figure 67: EMG and FSR Signals.

From their plots it can be seen concluded that both signals have a similar behaviour, since the muscle activity peaks are synchronized with each other. It can also be concluded that the muscle monitored contracts both in the flexion and extension of the respective joint. This indicates that both antagonist muscles work at the same time. While one muscles has a concentric contraction the other one has an eccentric contraction.

Table 12 represents the trials metrics results, such as the pearson correlation (C), which range of values goes from -1 (worst case) to 1 (best case), the delay between both signals which was calculated by measuring their cross-correlation, and their RMSE percentage.

Table 12: Static Trials Results.

Subjects	AT			Gastro			VL		
	C	Delay(s)	RMSE(%)	C	Delay(s)	RMSE(%)	C	Delay(s)	RMSE(%)
1	0.6	0.079	7.06	0.55	0.09	6.55	0.73	0.076	13.43
2	0.75	0.162	13.18	0.79	0.058	10.6	0.68	0.078	6.31
3	0.65	0.045	7.32	0.62	0.15	11.57	0.72	0.102	10.9

With these results it can be analysed that for all muscles, both signals are correlated, although the *gastrocnemius* showed the worst correlation result (subject 1) and some inconsistency between subjects correlation values. One of the main reasons for this behaviour is the delay between signals, which can decrease their correlation value.

These delays can be induced due the fact that the EMG signals happens before the FSR ones, and the fact of possible displacements between the electrodes and the FSR, being both positioned in different places in the same muscle, which have different activation times. Also the RMSE showed low values, with the worst scenario only having a RMSE of 13.43 %, indicating that both signals values are not very different from each other. To obtain these values first it was necessary to normalize the signals to the same scale, in order to obtain more realistic values.

In conclusion these results turned out to be quite satisfactory, indicating that, for these specific motions, the FSR sensors can contribute with similar EMG signals, providing enough information for the muscle activity monitoring in this scenario.

6.1.2 *Dynamic Trials*

In these trials the muscles activity monitoring was performed while the subject is walking, to validate the system while the subject is moving.

For these trials, it was used the EMG signal acquisition equipment from Delsys, which was available in the LABIOMEP. Figure 68 represents the LABIOMEP facilities and the Delsys equipment.

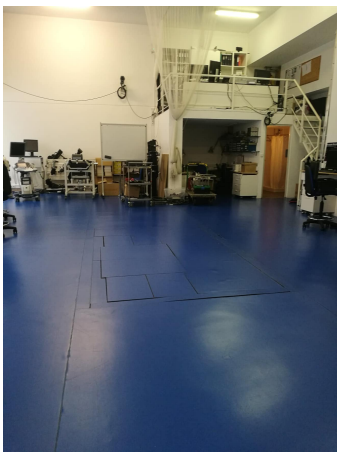

(a) Labiomep.

(b) Delsys EMG Signal Equipment (Delsys, 2018).

Figure 68: Labiomep Equipment.

To ensure a ground truth for helping synchronizing the data, two FSR sensors were placed in the toe and heel of the respective foot, as Figure 69 shows.

For the dynamic trials, the muscles monitored were the *anterior tibialis* and the *gastrocnemius*, since these muscles are the ones that contribute the most to the human gait. Three subjects participated in these trials, of both genders, different age (24.33 $\pm$ 0.58), weight (68.33 $\pm$ 12.42 Kg) and height (1.71 $\pm$ 0.12 m). These trials consist in walking in three different speeds: low pace, fast pace and a normal comfortable gait pace. Three trials were performed for each condition.

Figure 69: Foot FSR Location.

The FSR and EMG signals were acquired in sample frequencies of 100 Hz and 1 kHz respectively, so the EMG signal was later decimated to a frequency of 100 Hz. Since it was used different systems, it was needed to synchronize both *MuscLab* and the LABIOMEP systems. In the beginning and ending of each trial, the *MuscLab* sent a signal to the other system. The *Delsys* system output was the EMG raw signal, which contained lots of noise and negative values. So the signal was first rectified and then a butterworth second order low pass filter was applied with a cutoff frequency of 1.6 Hz. This process resulted in the signal available in Figure 70.

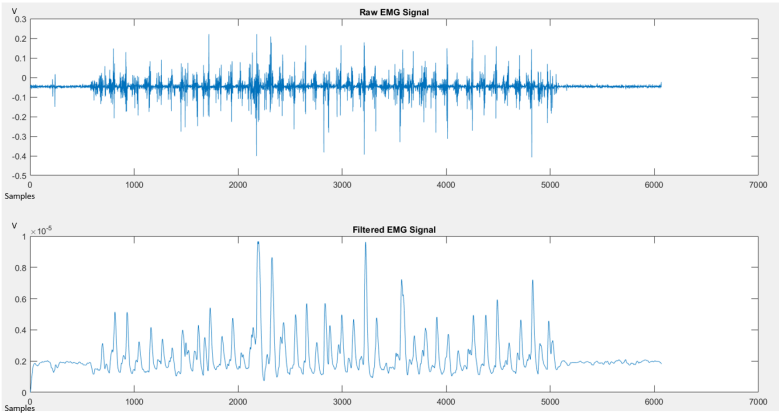

Figure 70: EMG Raw and Filtered Signals.

For these trials, the metrics validated were the delay between the signals, using the same process in the static trials and their RMSE values. Table 13 and Table 14 shows the delays and RMSE obtained in these trials respectively.

Table 13: Dynamic Trials Delays.

Subjects	AT			Gastro		
	Slow	Medium	Fast	Slow	Medium	Fast
1	0.29	0.007	0.33	0.22	0.03	0.6
2	-0.01	-0.45	0.12	0.15	0.47	-0.02
3	0.37	0.37	-0.28	0.02	-0.5	-0.14

Table 14: Dynamic Trials RMSE.

Subjects	AT			Gastro		
	Slow	Medium	Fast	Slow	Medium	Fast
1	30.13	28.68	25.87	36.53	43.5	24.27
2	18.92	30.19	33.55	23.77	37.88	23.45
3	15.92	18.47	26.62	26.26	25.34	26.10

In these trials the RMSE values were superior to the ones presented previously in the static trials. One of the main reasons that caused this difference is the fact that

these signals are less linear than the ones obtained in the static trials. Another main reason is the bigger delay between both signals.

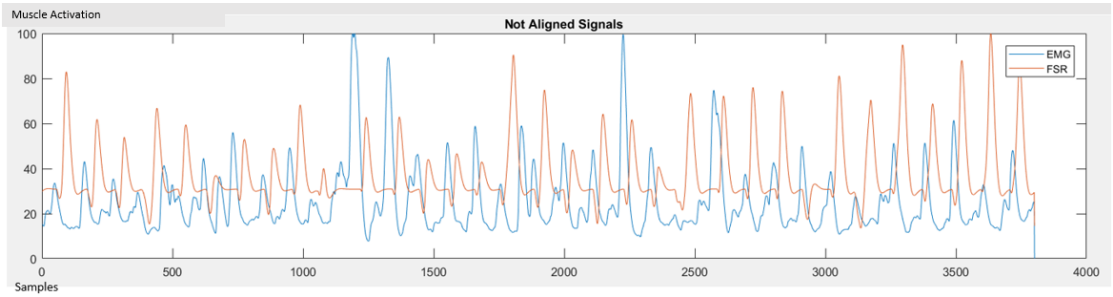

(a) Signals Not Aligned.

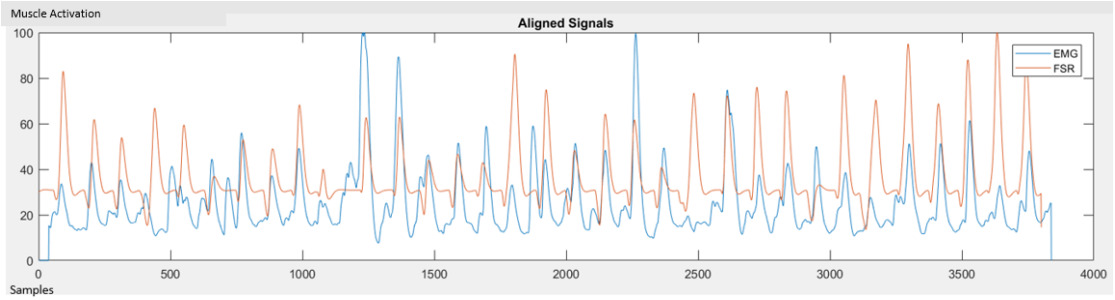

(b) Signals Aligned.

Figure 71: Dynamic Trial Plots.

The time delays were also superior to the ones measured in the previous trials. In this case, since the electrodes used from the *Delsys* system have bigger dimensions than the ones used in the static trials, it was not possible to insert the FSR sensors on top of the electrodes, so it was placed near the electrode. This induces a delay between both signals, because both muscle locations are activated in different times, as shown in Figure 71a. Also, some delays turned out to be negative because in some trials the FSR was anticipated to the EMG signal. After measuring the delays and RMSE between the signals, they were aligned in order to obtain more realistic correlation values (Figure 71b).

Due to the signals less linearity, two types of correlations were calculated: the pearson correlation which evaluates the linear relationship between two continuous variables, and the spearman correlation which evaluates the monotonic relationship between two continuous or ordinal variables (Minitab, 2018).

Both correlations were measured only in the instances when the corresponding muscle is activated and synchronized in both signals. So, a percentage of FSR

EMG synchronized peaks was also measured, as well as the mean of the magnitude difference between the EMG and the FSR maximum peaks value.

Table 15 represents the percentage of synchronized EMG FSR peaks, as well as the mean error between their maximum values.

Table 15: Dynamic Trials Peaks Comparison.

Subjects	AT						Gastro					
	Slow		Medium		Fast		Slow		Medium		Fast	
	Sync	Error	Sync	Error	Sync	Error	Sync	Error	Sync	Error	Sync	Error
1	67.67	25.4	67.33	14.35	81	16.06	87.67	20.68	66.67	23.62	72	17.72
2	71.33	-2.41	69.67	19.79	69.33	16.04	66	1.6	83	20.42	58	13.97
3	75.25	8.24	60.33	3.35	67.33	11.97	63.33	12.64	49.33	10.27	55.33	14.38

Some of the peaks maximum value error percentage turned out to be negative because the EMG signals maximum peak value turned out to be higher than the FSR ones. As for the amount of synchronized peaks percentage, the worst scenario just had 49.33 %, and the best scenario 81 %. This shows how much the sensors displacement regarding the electrodes can influence these results.

Table 16 shows the pearson correlation (CP) and the spearman correlation (CS). Both correlations showed similar results in most of the trials, and all of them showed that there was a strong correlation between the signals when the respective muscle is activated. This means that both signals have similar behaviours when the muscle is activated.

Table 16: Dynamic Trials Correlations.

Subjects	AT						Gastro					
	Slow		Medium		Fast		Slow		Medium		Fast	
	CP	CS	CP	CS	CP	CS	CP	CS	CP	CS	CP	CS
1	0.75	0.72	0.82	0.82	0.74	0.75	0.71	0.69	0.71	0.76	0.8	0.82
2	0.72	0.69	0.71	0.66	0.75	0.7	0.75	0.76	0.75	0.83	0.78	0.69
3	0.78	0.76	0.77	0.74	0.77	0.78	0.75	0.77	0.78	0.78	0.72	0.74

With these results, the **Research Question 1** (can the force sensors provide valid information to monitor muscle activity?) can be answered. Since in the FSR signals

it can be easily analysed when the respective muscle contracts and relaxes, and by comparing them with the EMG signals, which is the standard method for muscle monitoring and by these positive results which proved some similarities between them, yes the force sensing resistors can provide enough valid information for the muscle monitoring.

6.1.3 *Regression Models*

After validating the FSR signals, it was attempted to convert the FSR in EMG signals. To achieve this purpose, the relationship between both signals was studied and then several regression models were applied.

The regression models were estimated by using *MatLab* functions, such as normal linear regression and linear, quadratic and gaussian *Support Vector Regression (SVR)* models. SVR are very specific class of algorithms, characterized by usage of kernels, absence of local minima, sparseness of the solution and capacity control obtained by acting on the margin, or on number of support vectors, etc (Kernelsvm, 2018). These models were trained by introducing the raw FSR signals synchronized with the EMG filtered signals obtained in the previous dynamic trials, in the respective regression function, and then predict the final values based on the FSR data and compare the resulting data with the EMG signal. Figure 72 shows an example of both FSR and EMG signals inserted in the regression functions.

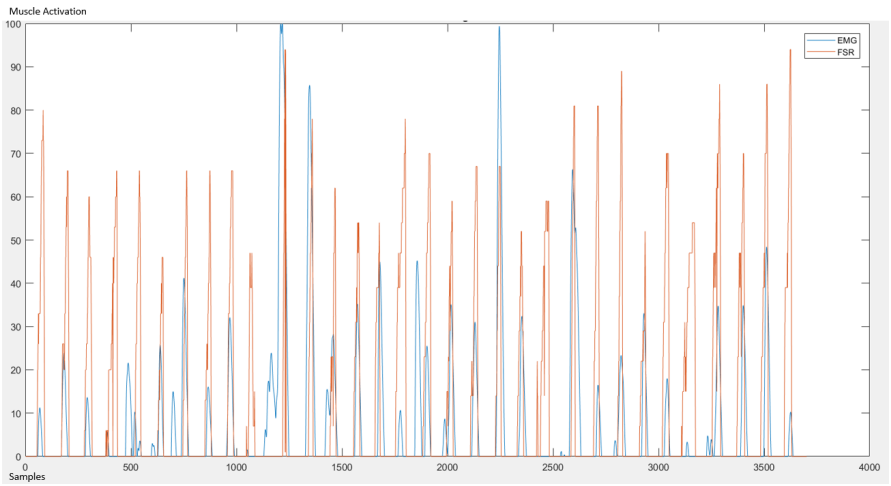

Figure 72: FSR and EMG Signals Regression Inputs.

For the signals presented in Figure 72, the linear normal regression was estimated, as well as the linear, quadratic and gaussian SVR models. Figure 73 shows the EMG values in the y axis with the FSR values in the x axis, as well as the models curves trying to establish a connection between the FSR and EMG values. Both signals do not share a pattern between them, so the models can not achieve the pretended behaviour. The gaussian SVR model also showed some overfit behaviour.

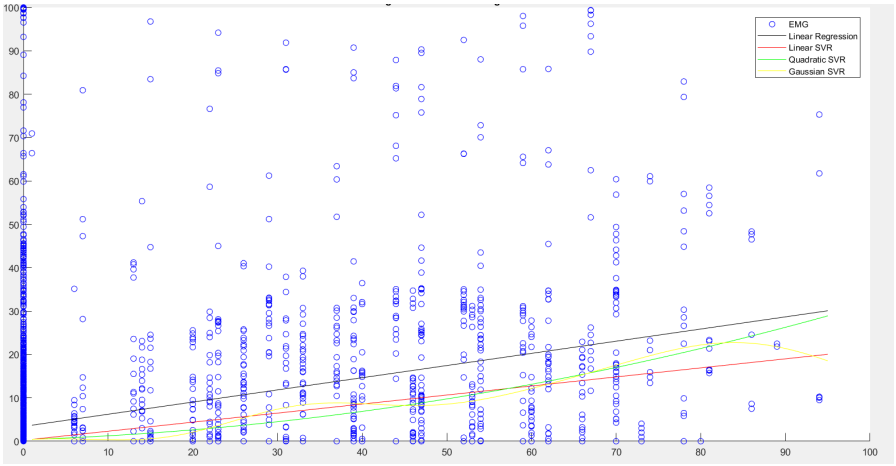

Figure 73: FSR and EMG Signals Regression Models.

Figure 74 represents the models predicaments to the FSR data along the trial. All models share similar behaviours, only changing the signal peaks values, although the normal linear regression model induces some offset between its signal peaks.

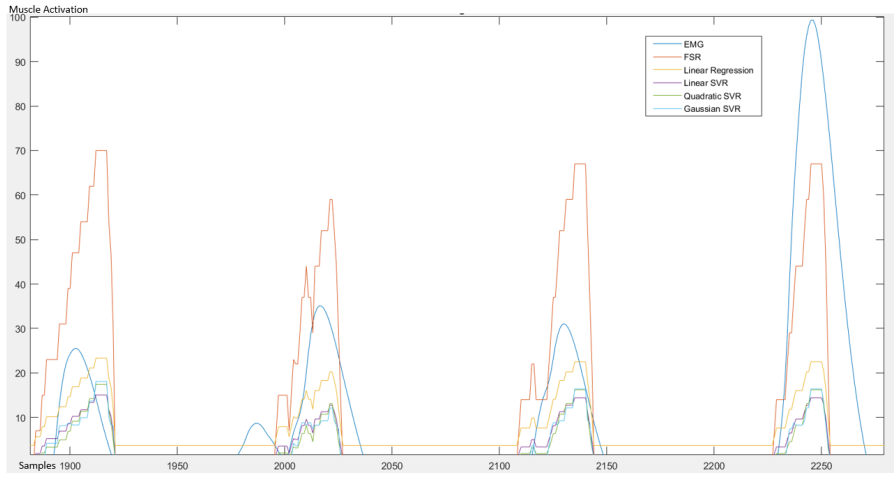

Figure 74: Regression Outputs.

Since this method didn't work, another approach was taken in action, that consisted repeating the previous method, but the signals inputs would be the signals peaks concatenated. Figure 75 shows the models curves trying to establish a pattern between the EMG points through the FSR values.

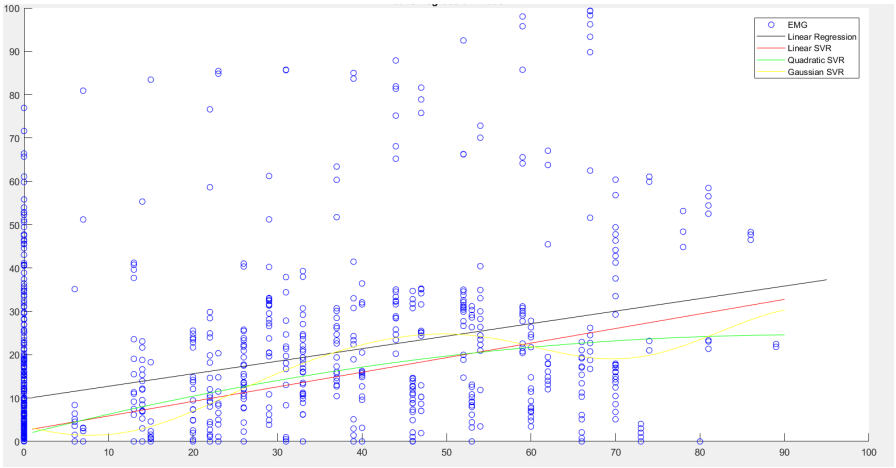

Figure 75: FSR and EMG Peaks Signals Regression Models.

In this scenario there isn't a pattern between both signals, leading to the estimation of unrealistic models, as Figure 76 shows.

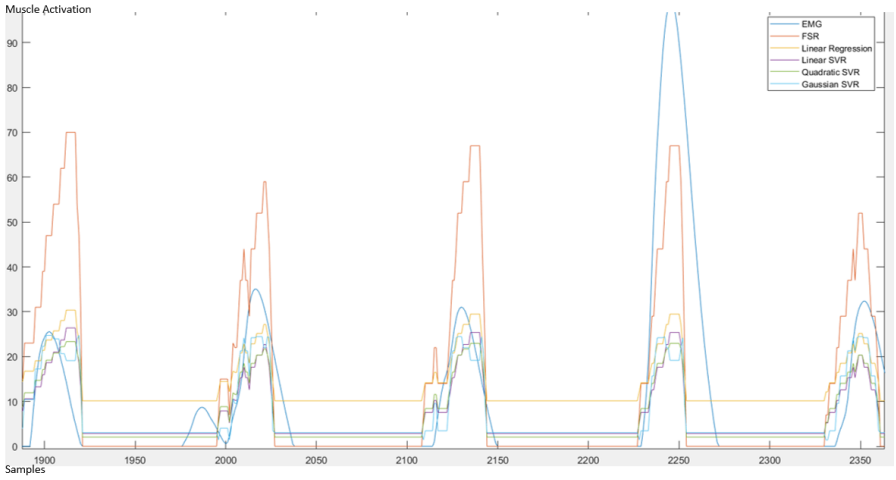

Figure 76: FSR and EMG Peaks Signals Regression Models.

This method was applied in 3 different trials of 3 different subjects, and the results were all similar. The model responses consisted only in increasing or decreasing

the signals peaks values, maintaining their wave forms. These results discarded the possibility of converting the FSR in EMG signals.

6.2 GAIT EVENT RECOGNITION VALIDATION

The gait event recognition algorithm was validated in the dynamic trials. The metrics measured in this validation was the algorithm accuracy and its delay. Table 17 sums up these metrics. The accuracy is displayed in % and the delay in ms.

Table 17: Toe-off Event Recognition Results

Subjects	Slow		Medium		Fast	
	Acc	Delay	Acc	Delay	Acc	Delay
1	82.67	0.34	80	-2.275	76	-1.11
2	56	-0.1	84	1.45	87	0.04
3	89	-5.72	82	-5.31	87.33	-4.34

There were only two scenarios in which the gait event recognition had an accuracy lower than 80 %. One of the main reasons why this happened was because of possible sensor displacements, not being able to acquire data correctly. In the remaining scenarios, the algorithm showed good results, displaying an accuracy between 82 % and 89 %. The delays which the algorithm took to recognize the gait event were also satisfactory, showing a maximum delay of 5.72 ms. The negative delay values mean that the algorithm detected the gait event before it really happened.

From these results, it can be concluded that with the signals provided by the FSR sensors, the toe-off gait event can be detected and recognized accurately, answering so the **Research Question 2** (is it possible to detect and recognize gait events through muscle activity provided from the force sensors?).

7

CONCLUSION

After this dissertation development, several conclusions could be achieved.

All the dissertation goals proposed were achieved successfully. An ergonomic and adaptive device was developed in order to monitor the muscle activity of a person, regardless its characteristics. Several projects were studied, in order to choose which sensor to use for monitoring the muscles, concluding that the FSR sensor would be the best choice due to its simplicity, small dimensions and its flexibility. The device hardware was also designed in order to contain small dimensions, in order to not cause discomfort in the subject, allowing him to move freely. The device hardware consists in 2 different interfaces: the battery interface, used to connect the battery to the MCU and use a voltage divider in order to analyse the battery output voltage by connecting its output to the microcontroller analogic pin, and the FSR sensor interface, used to connect the sensor to the MCU, consisting also in a voltage divider to acquire the sensor output and connect it to a low-pass filter, to ensure the signal does not contain aliasing. This design was also developed in a small PCB to ensure its ergonomics. The signal software calibration implemented in the device MCU also allows the system to automatically adapt to the subject wearing it, by withdrawing the signals offset and applying software gains accordingly to the subject's muscle stiffness, making the system versatile to every possible subject.

The muscle activity can also be monitored in real-time with the aid of a developed GUI and in offline mode, by reading the data saved in a memory card. The GUI allows the signal plots monitoring in real-time and displays also the sensors software gains estimated in the MCU signal calibration algorithm, as well as the current gait event detected. It also allows to check the battery charge level. This application is also able to save data in a file for future analysis, in case that option is enabled. The user can also run trials without the GUI aid, by running it in offline mode, with the device saving the data in a memory card inserted in it.

An algorithm was implemented in the microcontroller in order to detect and recognize the toe-off gait event based only in the data provided by the FSR data. The muscles monitored in order to detect it are the *anterior tibialis* and the *gastrocnemius*, due to their great influence in the human gait. This event is detected when the subject is already in the phase stance and both muscles relax, detecting the gait event, which also marks the transition from stance to swing phase.

Several protocols were established in order to validate the FSR signals and the toe-off gait event detection algorithm. The FSR signals were compared to the EMG signals, which is the standard method for muscle monitoring, and several metrics were studied. This comparison was made by performing trials in different condition with different subjects. This protocol was divided in 2 groups, such as the static trials where the subjects performs specific motions several times, and dynamic trials where the user walks in different paces with two FSR sensors placed in the subject's foot, one in the toe and the other in the heel. These trials were performed in different environments, using different EMG signal acquisition equipments. In the static trials, the FSR sensors were placed in top of the EMG electrodes. The metrics measured were the pearson correlation, the signals delay and their RMSE. These trials results showed that both signals presented good correlation between them, containing also small delays and low RMSE percentage, proving that they were similar. These trials also showed that both antagonists muscles responsible for a specific motion contract at the same time, one having a concentric contraction and the other an eccentric contraction. In the dynamic trials, different electrodes were used, containing bigger dimensions, needing to place the FSR sensors right next to the electrodes, in different places. For this reason, the signals acquired contained greater delays and RMSE, since they capture different muscle activation times, needing to align the signals acquired first in order to compare them, estimating the pearson and spearman correlations, and their peaks synchronized percentage, as well as their magnitude error. The peaks synchronized percentage values varied a lot, showing just how much the FSR and EMG sensors displacements can influence. As for the spearman and pearson correlations regarding the signals peaks, the trials showed strong correlations between them, proving that both signals have similar behaviours when the muscle is being activated. It was also attempted to convert the FSR signals in EMG signals, though normal regression models and SVR models. The results turned out to be negative, withdrawing this possibility.

As for the toe-off gait event detection algorithm validation, the algorithm was applied in the dynamic trials, with the FSR sensors placed in the subject's foot serving as a ground truth. The metrics estimated in this validation were the algorithm accuracy

and delay. The results proved to be satisfactory, with most of the trials showing accuracies higher than 80 % and the highest delay was 5.72 ms.

The system was also developed in order to function as a stand-alone product and was integrated in the *SmartOs* system, functioning as sensory subsystem. The modular programming and the fact that both microcontrollers being compatible by sharing the same hardware architecture made the integration process much easier. The functions responsible for acquiring and processing the FSR data and recognize the gait event were copied and adapted, discarding the other *MuscLab* system functions. The *MuscLab* board is supplied by the *SmartOs* board and the FSR output pins are connected to the *SmartOs* analogic pins.

7.1 RESEARCH QUESTIONS

Along the dissertation development, the research questions proposed were also answered.

Research Question 1: Can the force sensors provide valid information to monitor muscle activity? When validating the system by comparing the FSR with the EMG signal, it can be concluded that the FSR sensors provide enough information for muscle activity monitoring. Although the EMG signal can provide a more detailed monitoring, this process requires a much more complex electronics interface, and its raw data contains more noise than the FSR signal. By withdrawing the FSR signal offset it is easy to analyse when the muscle is activated though the signal peaks, and how much effort is being applied in those activations by also analysing the sensors software gains.

Research Question 2: Is it possible to detect and recognize gait events through muscle activity provided from the force sensors? Another conclusion taken from this dissertation development is that it is also possible to detect and recognize the toe-off event accurately from the FSR sensors positioned in the *anterior tibialis* and the *gastrocnemius* muscles. This algorithm was validated showing high accuracy values and low delays.

7.2 CONTRIBUTIONS

In this dissertation a wearable system was developed in order to monitor the subject's muscles activity, which can be useful in the sports area to improve an athlete's

performance, or in the medical rehabilitation area, functioning as a stand-alone project or as sensory system integrated in the *SmartOs* system.

This dissertation proved that it is possible to monitor the muscles activity without the need of expensive resources like the EMG signal acquisition requires, which is the standard method for muscle monitoring. In the *MuscLab* system only a voltage divider and a low-pass filter was needed to acquire the FSR sensor output. The FSR sensors allow the muscle monitoring without the need of a specific gel or hairless hair, becoming a more independent tool than the EMG electrodes sensors. They can also be easily integrated in a wearable system due to their flexibility and simplicity, not needing complex electronics and signal processing as the EMG signal acquisition requires, allowing to design and develop a system hardware containing fewer components and more reduced dimensions, allowing it to be more practical and cheaper.

7.3 FUTURE WORK

One possible future system update is to integrate the FSR sensors in textiles, improving the system ergonomics. One of the FSR main advantages is their flexibility and how easily they can be integrated in textiles, allowing the muscle monitoring in a more ergonomic way. The possibility of switching the device PCB to a *Flexible Printed Circuit Board (FPCB)* could also be studied, so that the device hardware could also be integrated in clothes, discarding the need of the cases developed and allow the user to feel more comfortable. These improvements would increase significantly the device ergonomics and efficiency, allowing it to become a very useful tool to be used in the medical rehabilitation area and also in the sports area.

BIBLIOGRAPHY

AceFitness. Muscles That Move the Leg, 2018. URL https://www.acefitness.org/fitness-certifications/resource-center/exam-preparation-blog/3594/muscles-that-move-the-leg.

Oliver Amft, Holger Junker, Paul Lukowicz, Gerhard Tröster, and Corina Schuster. Sensing muscle activities with body-worn sensors. *Proceedings - BSN 2006: International Workshop on Wearable and Implantable Body Sensor Networks*, 2006:138–141, 2006. doi: 10.1109/BSN.2006.48.

Jonas Beil, Gernot Perner, and Tamim Asfour. Design and Control of the Lower Limb Exoskeleton KIT-EXO-1. *International Conference on Rehabilitation Robotics (ICORR)*, pages 119–124, 2015. ISSN 1945-7898. doi: 10.1109/ICORR.2015.7281186.

BotnRoll. Hacker LiPoBattery 7.4 V / 900mAh - botnroll.com, 2018. URL http://www.botnroll.com/pt/baterias-e-carregadores/1052-hacker-lipobattery74-v-900mah.html.

Botnroll. Módulo Bluetooth HC06 - botnroll.com, 2018. URL https://www.botnroll.com/pt/bluetooth/2583-m-dulo-bluetooth-hc06.html?search_query=hc06&results=2.

Delsys. Trigno EMG Systems — Delsys, Inc., 2018. URL https://www.delsys.com/products/wireless-emg/.

ELPROCUS. Force Sensing Resistor - How it Works and its Applications, 2017. URL https://www.elprocus.com/force-sensing-resistor-technology/.

O. Ethgen, C. Beaudart, F. Buckinx, O. Bruyère, and J. Y. Reginster. The Future Prevalence of Sarcopenia in Europe: A Claim for Public Health Action. *Calcified Tissue International*, 100(3):229–234, 2017. ISSN 14320827. doi: 10.1007/s00223-016-0220-9.

Joana Figueiredo, Cesar Ferreira, Luis Costa, Joao Sepulveda, Luis P. Reis, Juan C. Moreno, and Cristina P. Santos. Instrumented insole system for ambulatory and

robotic walking assistance: First advances. *2017 IEEE International Conference on Autonomous Robot Systems and Competitions, ICARSC 2017*, pages 116–121, 2017. doi: 10.1109/ICARSC.2017.7964062.

GearBest. HC - 06 Wireless Bluetooth Transceiver Module - $4.29 Free Shipping—GearBest.com, 2018. URL https://www.gearbest.com/sensors/pp{_}241478.html.

Bang good. 9 Pin Micro SD TF Storage Card Board Memory Shield Module For Arduino Sale - Banggood.com sold out, 2018. URL https://www.banggood.com/9-Pin-Micro-SD-TF-Storage-Card-Board-Memory-Shield-Module-For-Arduino-p-1064191.html?cur{_}warehouse=CN.

Bret H Goodpaster, Seok Won Park, Tamara B Harris, Steven B Kritchevsky, Michael Nevitt, Ann V Schwartz, Eleanor M Simonsick, Frances A Tylavsky, Marjolein Visser, and Anne B Newman. The loss of skeletal muscle strength, mass, and quality in older adults: the health, aging and body composition study. *Journal of Gerontology: MEDICAL SCIENCES*, 61(10):1059–64, 2006. ISSN 1079-5006. doi: 10.1093/gerona/61.10.1059.

Pyeong-gook Jung, Student Member, Gukchan Lim, and Seonghyok Kim. A Wearable Gesture Recognition Device for Detecting Muscular Activities Based on Air-Pressure Sensors. 11(2):485–494, 2015.

Kernelsvm. Support Vector Machine Regression, 2018. URL http://kernelsvm.tripod.com/.

Kyung Kim, Chang Ho Yu, Gu Young Jeong, Min Heo, and Tae Kyu Kwon. Analysis of the assistance characteristics for the knee extension motion of knee orthosis using muscular stiffness force feedback. *Journal of Mechanical Science and Technology*, 27(10): 3161–3169, 2013. ISSN 1738494X. doi: 10.1007/s12206-013-0837-9.

Matthias Kreil, Georg Ogris, and Paul Lukowicz. Muscle activity evaluation using force sensitive resistors. *2008 5th International Summer School and Symposium on Medical Devices and Biosensors*, pages 107–110, 2008. doi: 10.1109/ISSMDBS.2008.4575029. URL http://ieeexplore.ieee.org/lpdocs/epic03/wrapper.htm?arnumber=4575029.

Kyoungchul Kong and Doyoung Jeon. Fuzzy Control of a New Tendon-Driven Exoskeletal Power Assistive Device. *Proceedings, 2005 IEEE/ASME International*

Conference on Advanced Intelligent Mechatronics., pages 146–151, 2005. doi: 10.1109/AIM.2005.1500981. URL http://ieeexplore.ieee.org/lpdocs/epic03/wrapper.htm?arnumber=1500981.

Paul Lukowicz, T Kirstein, and G Tröster. Wearable systems for health care applications. *Methods of Information in Medicine*, 43(3):232–238, 2004. ISSN 00261270. doi: 10.1267/METH04030232.

Paul Lukowicz, Friedrich Hanser, Christoph Szubski, and Wolfgang Schobersberger. *Detecting and Interpreting Muscle Activity with Wearable Force Sensors*. 2009. ISBN 9783642046667. URL http://www.ulb.tu-darmstadt.de/tocs/79304567.pdf.

MakerBright. Interlink 406 Force-Sensing Resistor Square - 0.2N to 20N Sensitivity, 2018. URL https://www.makerbright.com/interlink-fsr-406-force-sensing-resistor-1-5-square.html.

Jan Meyer, Paul Lukowicz, and Gerhard Troster. Textile Pressure Sensor for Muscle Activity and Motion Detection. *Iswc*, pages 69–72, 2006. ISSN 1550-4816. doi: 10.1109/ISWC.2006.286346.

Minitab. A comparison of the Pearson and Spearman correlation methods, 2018. URL https://support.minitab.com/en-us/minitab-express/1/help-and-how-to/modeling-statistics/regression/supporting-topics/basics/a-comparison-of-the-pearson-and-spearman-correlation-methods/.

Georg Ogris, Matthias Kreil, and Paul Lukowicz. Using FSR based muscule activity monitoring to recognize manipulative arm gestures. *Proceedings - International Symposium on Wearable Computers, ISWC*, pages 45–48, 2007. ISSN 15504816. doi: 10.1109/ISWC.2007.4373776.

Olimex. ECG-GEL-ELECTRODE, 2018. URL https://www.olimex.com/Products/Modules/Biofeedback/ECG-GEL-ELECTRODE/.

Ferenc Preisach. Über die magnetische Nachwirkung am Carbonyleisen. *Annalen der Physik*, 421(7):605–635, 1937. ISSN 15213889. doi: 10.1002/andp.19374210705.

Qt. Libraries; APIs, Tools and IDE — Qt, 2018. URL https://www.qt.io/qt-features-libraries-apis-tools-and-ide/.

J. Rekimoto. GestureWrist and GesturePad: unobtrusive wearable interaction devices. *Proceedings Fifth International Symposium on Wearable Computers*, pages 21–27, 2001.

ISSN 1530-0811. doi: 10.1109/ISWC.2001.962092. URL http://ieeexplore.ieee.org/document/962092/.

STMicroelectronics. NUCLEO-F303K8 - STM32 Nucleo-32 development board with STM32F303K8 MCU, supports Arduino connectivity - STMicroelectronics, 2018a. URL http://www.st.com/en/evaluation-tools/nucleo-f303k8.html/{#}design-scroll.

STMicroelectronics. STM32F4DISCOVERY - Discovery kit with STM32F407VG MCU * New order code STM32F407G-DISC1 (replaces STM32F4DISCOVERY) - STMicroelectronics, 2018b. URL https://www.st.com/en/evaluation-tools/stm32f4discovery.html.

STMicroelectronics. STM32CubeMX - STM32Cube initialization code generator - STMicroelectronics, 2018c. URL http://www.st.com/en/development-tools/stm32cubemx.html.

Yan Wang, Li Wang, Tingting Yang, Xiao Li, Xiaobei Zang, Miao Zhu, Kunlin Wang, Dehai Wu, and Hongwei Zhu. Wearable and highly sensitive graphene strain sensors for human motion monitoring. *Advanced Functional Materials*, 24(29): 4666–4670, 2014. ISSN 16163028. doi: 10.1002/adfm.201400379.

Zhen G Xiao and Carlo Menon. Towards the development of a wearable feedback system for monitoring the activities of the upper-extremities. *Journal of NeuroEngineering and Rehabilitation*, 11(1):2, 2014. ISSN 1743-0003. doi: 10.1186/1743-0003-11-2. URL http://jneuroengrehab.biomedcentral.com/articles/10.1186/1743-0003-11-2.

Enhao Zheng, Baojun Chen, Kunlin Wei, and Qining Wang. Lower limb wearable capacitive sensing and its applications to recognizing human gaits. *Sensors (Basel, Switzerland)*, 13(10):13334–13355, 2013. ISSN 14248220. doi: 10.3390/s131013334.